Preliminary Earthquake Reconnaissance Report:

Türkiye Earthquake Sequence on

February 6, 2023

Field Assessment Team Lead
Gulen Ozkula

Field Reconnaissance Assessment Team Authors
(in alphabetical order)

Tugce Baser, University of Illinois at Urbana Champaign	Jui-Liang Lin, National Center for Research on Earthquake Engineering (NCREE)
Robert K. Dowell, San Diego State University	Ozgun A. Numanoglu, Schnabel Engineering
Ayse Hortacsu, Applied Technology Council	C. Guney Olgun, Missouri University of Science and Technology
Cheng-Wei Huang, National Center for Research on Earthquake Engineering (NCREE)	Tunc Deniz Uludag, Martin/Martin Engineering
Okan Ilhan, Ankara Yildirim Beyazit University	

April 2023

ACKNOWLEDGEMENTS

We extend our sincere appreciation and gratitude to all the individuals and organizations who contributed their time, effort, and expertise in conducting the post-earthquake reconnaissance. We are particularly grateful to the locals in the region who shared their experiences with us and helped us understand the significance of the earthquake.

We also extend our thanks to Eylem Ulutas Ayatar, President of the Turkish Civil Engineering Association, Izmir Branch, for providing us with the necessary permissions, as well as to Ercan Acimis and Mehmet Kiliclar, who are members of the Organized Industrial Zone (OIZ).

We recognize the critical importance of conducting post-earthquake reconnaissance to observe, document, and analyze the seismic performance of built and natural environments. Although laboratory experiments and analytical modeling are valuable, post-earthquake reconnaissance provides the ultimate test of our progress in mitigating the effects of natural hazards on society.

All the authors and editors listed on the cover page of this report participated as volunteer professionals. Therefore, any opinions, findings, conclusions, or recommendations expressed herein are those of the individual contributors and do not necessarily reflect the views of their employer or any other institutions or organizations with which they are affiliated.

EXECUTIVE SUMMARY

On February 6th, 2023, a M_w 7.8 earthquake hit southern Türkiye at 4:17 am (local time), followed by a M_w 7.5 earthquake in the same region about 9 hours later, at 1:24 pm (local time). The epicentral coordinates reported by both the U.S. Geological Survey (USGS, 2023) and the AFAD Seismological Center (Disaster and Emergency Management Presidency, 2023) were 37.288°N, 37.043°E for the M_w 7.8 event. The USGS reported a hypocenter depth of 10.0 km for both events, whereas the AFAD Seismological Center reported a depth of 8.6 km for the mainshock. There have been several earthquakes of magnitude 6.0 and larger in the sequence (USGS, 2023). Earthquake sequences with consequent large magnitude events separated by short time intervals have been occurring at different parts of the world in the past years (e.g., 2019 Ridgecrest earthquakes (Mosalam et al., 2019); 2022 Iran earthquake sequence (Mosalam et al., 2022), 2022 Taiwan earthquake sequence (Mosalam et al., 2022)). From a structural engineering and design perspective, this is a reminder that strong pre-shocks and aftershocks (even with the same magnitude) can occur before and after the mainshock and their cumulative effects should be characterized and considered in the design codes of buildings and other infrastructure systems.

As a result of this unprecedented series of back-to-back earthquakes, in populated regions, damage was observed for residential buildings, industrial structures, bridges, transportation systems, earth structures, harbors and lifelines, with direct infrastructure loss exceeding $34 billion according to initial estimates (World Bank, 2023). In addition to strong ground sharing in the near-field, one of the root causes that exacerbated this natural hazard into a catastrophic disaster was the large ground deformations such as landslides, fault rupture, and ground subsidence which severely affected critical infrastructure including lifelines and roads. The cities affected most by these sequential earthquakes are Kahramanmaras, Adiyaman, Hatay, Osmaniye, Gaziantep, Malatya, Adana, Diyarbakir, Elazig and Kilis with residents of over 15 million (which constitute about 17% of Türkiye's population). According to official records, the number of fatalities was about 50,000 and more than 100,000 people were injured. A total of 19,284 buildings in ten different cities collapsed and 373,038 buildings were reported as damaged to different levels (Ministry of Environment, Urbanization and Climate Change, 2023).

TABLE OF CONTENTS

1 INTRODUCTION

1.1 Introduction

On February 6th, 2023, a M_w 7.8 earthquake hit southern Türkiye at 4:17 am (local time), followed by a M_w 7.5 earthquake in the same region about 9 hours later, at 1:24 pm (local time). The epicenter of the first earthquake was located at 37.288°N and 37.043°E, with a focal depth of 10 km, while the second earthquake's epicenter was about 175 km away from the first one, located at 38.089°N and 37.239°E, also with a focal depth of 10 km. These back-to-back earthquakes caused significant damage to the populated regions, including residential buildings, industrial structures, bridges, transportation systems, earth structures, harbors, and lifelines, with initial estimates suggesting direct infrastructure losses exceeding $34 billion (World Bank, 2023). The cities most affected by these sequential earthquakes are Kahramanmaras, Adiyaman, Hatay, Osmaniye, Gaziantep, Malatya, Adana, Diyarbakir, Elazig, and Kilis, with a combined population of over 15 million people, which constitutes about 17% of Türkiye's population. According to official records, the earthquakes caused about 50,000 fatalities, more than 100,000 injuries, and the collapse of 19,284 buildings in ten different cities. Additionally, 373,038 buildings were reported as damaged to different degrees (Ministry of Environment, Urbanization and Climate Change, 2023).

The team was strategically divided into two specialized groups. The first group, consisting of geotechnical experts, arrived in the affected region on February 11th, a week after the incident. The second group, focusing on structural assessments, reached their base in Adana, Southern Türkiye, on February 19th, two weeks following the earthquake sequence. This timing allowed the structural team to commence their work right after the search and rescue operations were concluded, and before the majority of damaged or failed structures were demolished and removed. The team conducted thorough investigations in several towns and cities, including Iskenderun, Antakya, Osmaniye, Kahramanmaras, Gaziantep, Nurdagi, Golbasi, and Antakya (see Figure 1-1), with the primary objective of collecting and documenting time-sensitive data related to structural damage and geotechnical impacts. Their investigative efforts were mainly centered on documenting the region's geology, seismo-tectonics, geological field observations, seismological background, and processing of strong ground motion records. In addition, the team meticulously documented the performance of various structures and infrastructures, such as residential buildings, bridges, building foundations, soil and rock slopes, manifestations of seismic soil liquefaction, rockfalls, earth dams, harbors, lifelines, ports, deep excavations, retaining structures, and industrial facilities. It is important to acknowledge that the conclusions drawn by the authors in this report are preliminary in nature. Subsequent research and analysis of the collected data are expected to yield more comprehensive and definitive insights into the observations presented herein.
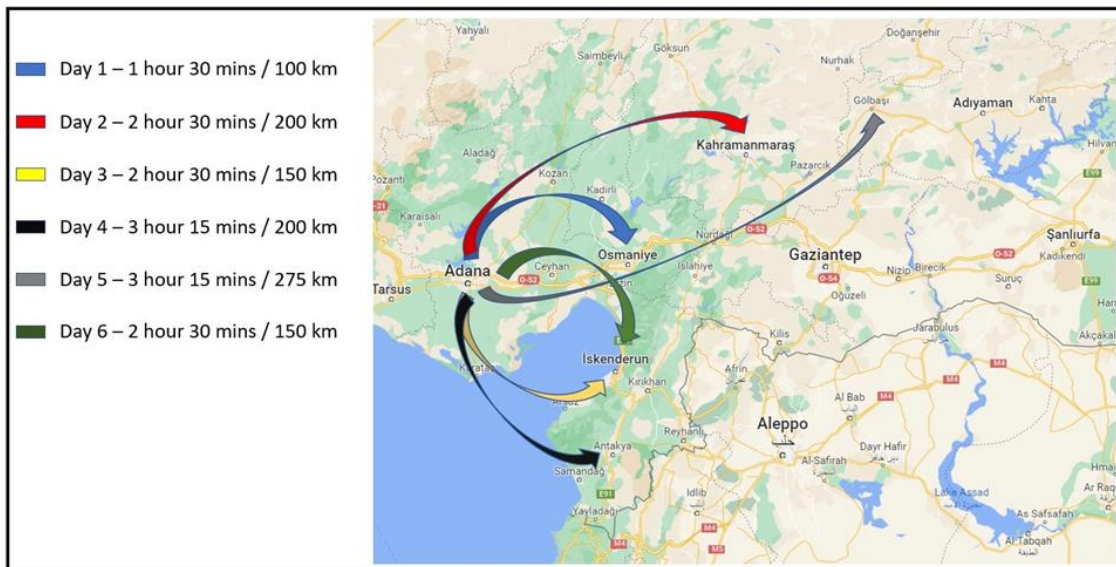

Figure 1-1 Route for Reconnaissance Tour

Team members included:

Gulen Ozkula, Department of Civil and Environmental Engineering, University of Wisconsin, Platteville, WI 53818, USA

Tugce Baser, Department of Civil and Environmental Engineering, University of Illinois at Urbana Champaign, IL, USA

Robert K. Dowell, Department of Civil, Construction, and Environmental Engineering, San Diego State University, San Diego, CA, 92182, USA

Ayse Hortacsu, Applied Technology Council, San Francisco, USA

Cheng-Wei Huang, National Center for Research on Earthquake Engineering, Taipei, Taiwan

Okan Ilhan, Department of Civil Engineering, Ankara Yildirim Beyazit University, Ankara, Türkiye

Jui-Liang Lin, National Center for Research on Earthquake Engineering, Taipei, Taiwan

Ozgun A. Numanoglu, Schnabel Engineering, Seattle, WA 98188, USA

C. Guney Olgun, Department of Civil, Architectural and Environmental Engineering, Missouri University of Science and Technology, Rolla, MO 65409, USA

Tunc Deniz Uludag, Martin / Martin Engineering, Lakewood, CO 80215, USA

2 SEISMICITY

2.1 Strong Ground Motions

The East Anatolian Fault Zone (EAFZ) is known to be seismically active due to its extrusion between stable Eurasian and Arabian plates, where the latter moves towards the northeast relative to the Anatolian plate (Cetin et al., 2023) with 18-25 mm/year, leading to a horizontal slip rate of 9 ∓ 1 mm/year and 10-20 mm/year in the North Anatolian Fault Zone (NAFZ) and EAFZ (Nalbant et al, 2002; Cetin et al., 2003). Considering this movement of EAFZ, many historical records that describe the events and damaged areas such as the earthquakes that occurred on 1114, 11th October 1138, 1269, 1344, 1514, 1544, 1795 (Sesetyan et al., 2023) and the Elazig earthquake on January 24th, 2020, with M_w = 6.8 lend credence to the potential of the EAFZ to produce large magnitude events. On February 6th, 2023, at 01:17:34 (UTC), an earthquake with epicenter at 37.225°N 37.021°E (26 km east-northeast of Nurdagi, Gaziantep), with moment magnitude (M_w) of 7.8, and depth of 10.0 km struck Türkiye (USGS, 2023a). Figure 2-1 illustrates the ruptured fault (in red), which is composed of Erkenek, Pazarcik and Amanos fragments of EAFZ and produced a strike-slip movement with a length of approximately 290 km (Hancilar et al., 2023), resulting in the M_w 7.8 earthquake. As stated in Cetin et al. (2023) and illustrated in Figure 2-2, the fault movement is bilateral; it is initiated by a rupture in the Narli fault (in the direction of blue arrow in Figure 2-2) and is followed by movement from Pazarcik to Erkenek in the north-east direction (yellow arrow in Figure 2-2), as well as rupture throughout the Amanos segment (green arrow in Figure 2-2), after some delay.

After ~10 minutes (February 6th, 2023, 01:28:15 UTC) from the first event, an earthquake with epicenter at 37.189°N 36.893°E (14 km East of Nurdagi, Türkiye), with M_w of 6.7 and depth of 9.8 km depth shook the area (USGS, 2023b). It is thought that the earthquake that occurred ~9 hours from the first event (February 6th, 2023, at 10:24:49 UTC), with epicenter at 38.024°N 37.203°E (4 km south-southeast of Ekinozu, Kahramanmaras) and with M_w of 7.5 and depth of 10.0 km (USGS, 2023c) was triggered by these two earthquakes. Analogous to the M_w 7.8 earthquake, the moment tensor solution of M_w of 7.5 event exhibited in Figure 2-1 (in yellow) indicates a strike-slip movement consistent with the EAFZ fault mechanism. Cetin et al. (2023) estimated a 160 km rupture length from Cardak fault towards Dogansehir (Malatya) fault zone with observed surface displacements ranging from 2 to 8 m.
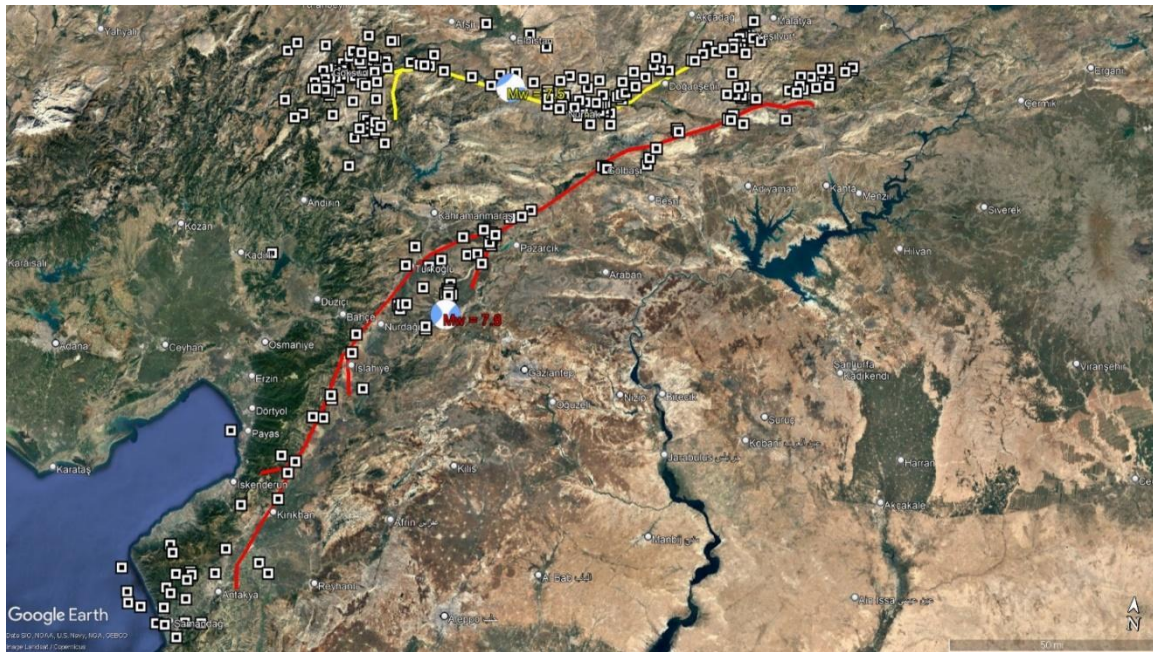

Figure 2-1 The fault ruptures and epicenter locations of M_w 7.8 and M_w 7.5 earthquakes (The beach ball diagrams representing the focal mechanism were downloaded from USCS (2023a) and USCS (2023b)) along with the aftershocks.
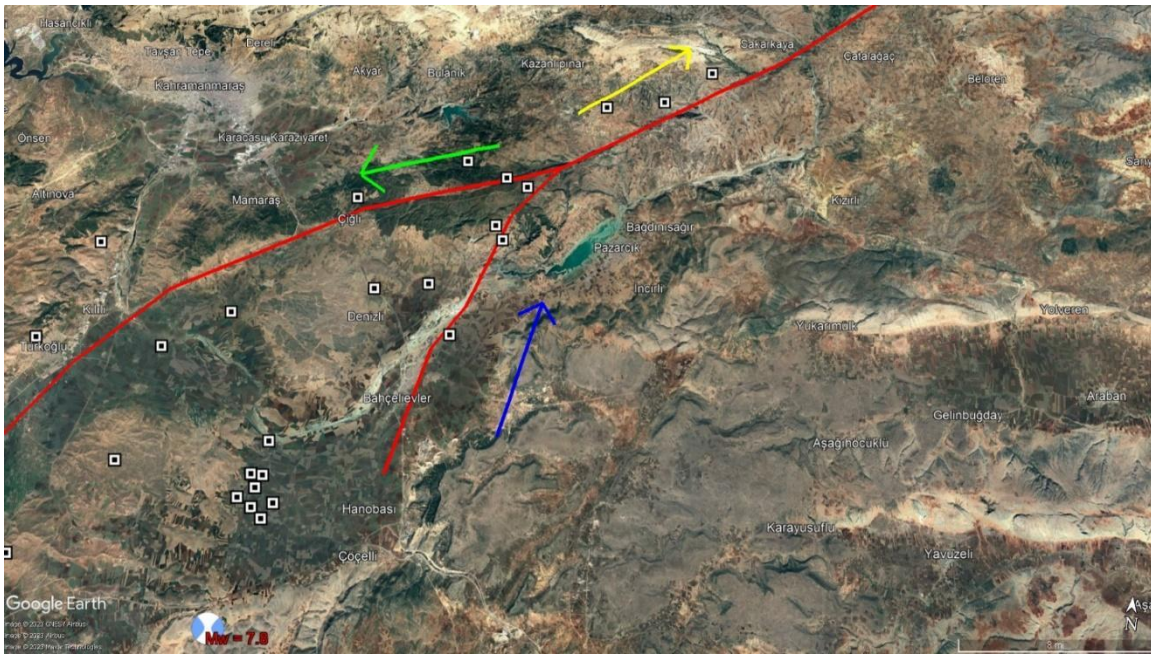
Figure 2-2 The fault rupture propagation of M_w 7.8 earthquake

2.2   Strong Ground Motion Data Process

The events of M_w 7.8 and M_w 7.5 were recorded at 290 and 267 stations of the AFAD (Disaster and Emergency Presidency of Türkiye), respectively. All these motions were downloaded as raw acceleration data to be compared with design spectra suggested by Turkish Earthquake Building Code (TEBC, 2019) and were subjected to a visual check to detect long period noise ($\geq$ 0.1 Hz), which can be identified through (i) velocities that do not approach the value of zero at the end of the record (Akkar and Boore, 2009), or (ii) displacement time histories which exhibit wobbles or significant shifts from the zero line. Figure 2-3(a) illustrates the raw acceleration time-history (TH) recorded by Station 3802 during the M_w 7.5 event. The wavering observed in velocity TH calculated through cumulative summation of acceleration TH indicates the long-period noise in raw acceleration data, leading to larger and unrealistic values in displacement TH.
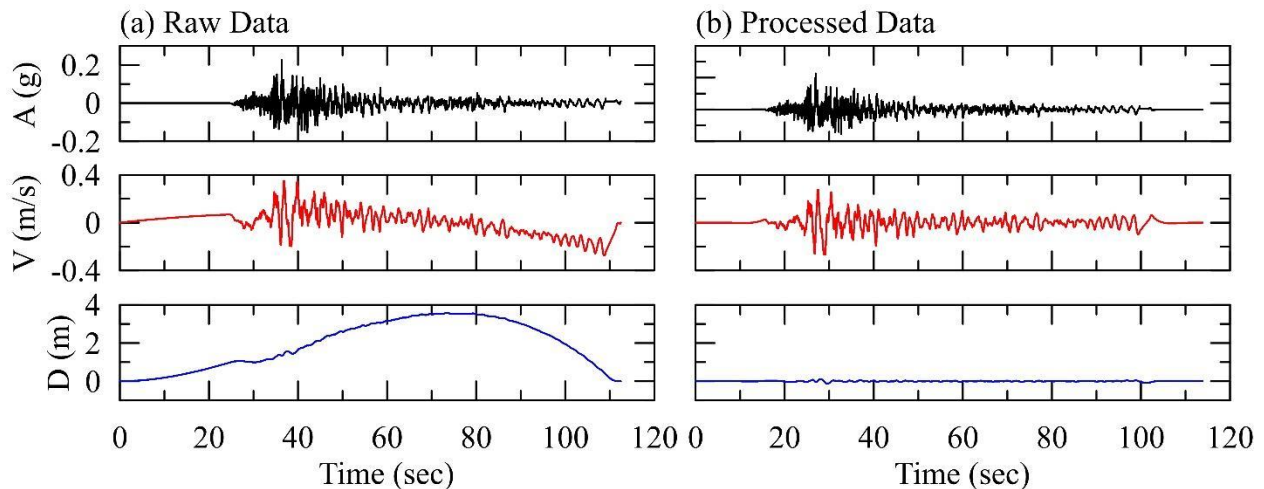
Figure 2-3 The (a) raw and (b) processed acceleration (A), velocity (V) and displacement (D) time histories recorded at station 3802 during the M_w 7.5 earthquake.

This issue of contaminated acceleration data due to long-period noise was resolved through the ground motion processing approach of BAP (Basic Strong-Motion Accelerogram Processing Software), which is proposed in Converse and Brady (1992) and is implemented in DEEPSOIL V7.0 (Hashash et al., 2020) through the "Baseline Correction" option in DEEPSOIL v7.0. Figure 2-3 presents the application of baseline correction to raw acceleration data in that (a) the downward slope and offset in velocity TH in Figure 2-3(a) is removed, and (b) the unrealistic displacement trend in Figure 2-3(b) is corrected.

2.3   Comparison of Spectral Curves at Selected Stations with TEBC (2019) Design Spectrum

Figure 2-4 compares recorded THs, response spectral accelerations and design spectra required by the Turkish Earthquake Building Code (TEBC, 2019) for return periods of 2475 years (exceedance probability of 2% in 50 years) and 475 years (exceedance probability of 10% in 50 years) for rock-like material (V_{S30} > ~600-700 m/s) and soil sites for the M_w 7.8 event. For Station 4611 (V_{S30} = 731 m/s and rupture distance (R_{RUP}) of 16.9 km) located in the city of Kahramanmaras, the PGA values for E-W and N-S components are 0.32 and 0.35 g, respectively, and the spectral accelerations (SA) of two horizontal components are consistent with the TEBC (2019)-475 years design spectrum. In the case of Station 4616 located at a soil site (V_{S30} = 390 m/s and R_{RUP} = 2.34 km) in Kahramanmaras, the recorded PGAs for E-W and N-S components increase to the values of 0.51 g and 0.67 g, respectively, comparted to Station 4611, and the spectral curves of recorded ground motions reach the TEBC (2019)-2475 years spectrum at oscillator periods (T_{OSC}) of ~0.5 s, ~0.75 s and 1.5 s. Two conditions are thought to lead to this observation: (i) closer distance to rupture plane for Station 4616 relative to Station 4611, and (ii) site effects (Seed et al., 1988). The influence of site on strong ground motion is more pronounced for the city of Hatay, where SA values from Station 3135 (V_{S30} = 460 m/s and R_{RUP} = 34.21 km) exceed the TEBC (2019) - 2475 years spectrum for T_{OSC} ≤ 1.0 sec, but SAs of motions recorded in Station 3116 (V_{S30} = 870 m/s and R_{RUP} = 17.43 km) are on the order of TEBC (2019) - 475 years spectrum.

The analogous evaluation described above is performed using the recorded motions from two stations in Kayseri during the M_w 7.5 event, as illustrated in Figure 2-5. Even though the SA values of motions at Station 3804 (V_{S30} = 637 m/s, R_{RUP} = 77.77 km) lie notably beneath the TEBC (2019) – 475 years spectrum, Station 3802 (V_{S30} = 305 m/s, R_{RUP} = 49.33 km) is thought to have significant site amplification, leading to the exceedance of SA values for the E-W component to the TEBC (2019) – 2475 years spectrum for 2.0 sec ≤ T_{OSC} ≤ 2.5 sec. The similar phenomenon is observed in the case where the spectral accelerations from Station 4611 (V_{S30} = 731 m/s, R_{RUP} = 28.62 km) and from Station 4612 (V_{S30} = 246 m/s, R_{RUP} = 3.19 km) are compared in that the latter significantly exceeds the TEBC (2019) – 2475 years spectrum for 1.0 sec ≤ T_{OSC} ≤ 2.0 sec.

Figure 2-4 The baseline corrected acceleration (A) time histories in (a) E-W, (b) N-S directions, and (c) 5% damped response spectral accelerations (SA) and design spectra suggested by TEBC (2019) for return periods of 2475 years and 475 years for station ID of 4611 located in Kahramanmaras. The same information is presented for (d, e, f) station ID of 4616, (g, h, i) station ID (Hatay) of 3116, and (j, k, l) station ID (Hatay) of 3135 (M_w = 7.8 event).
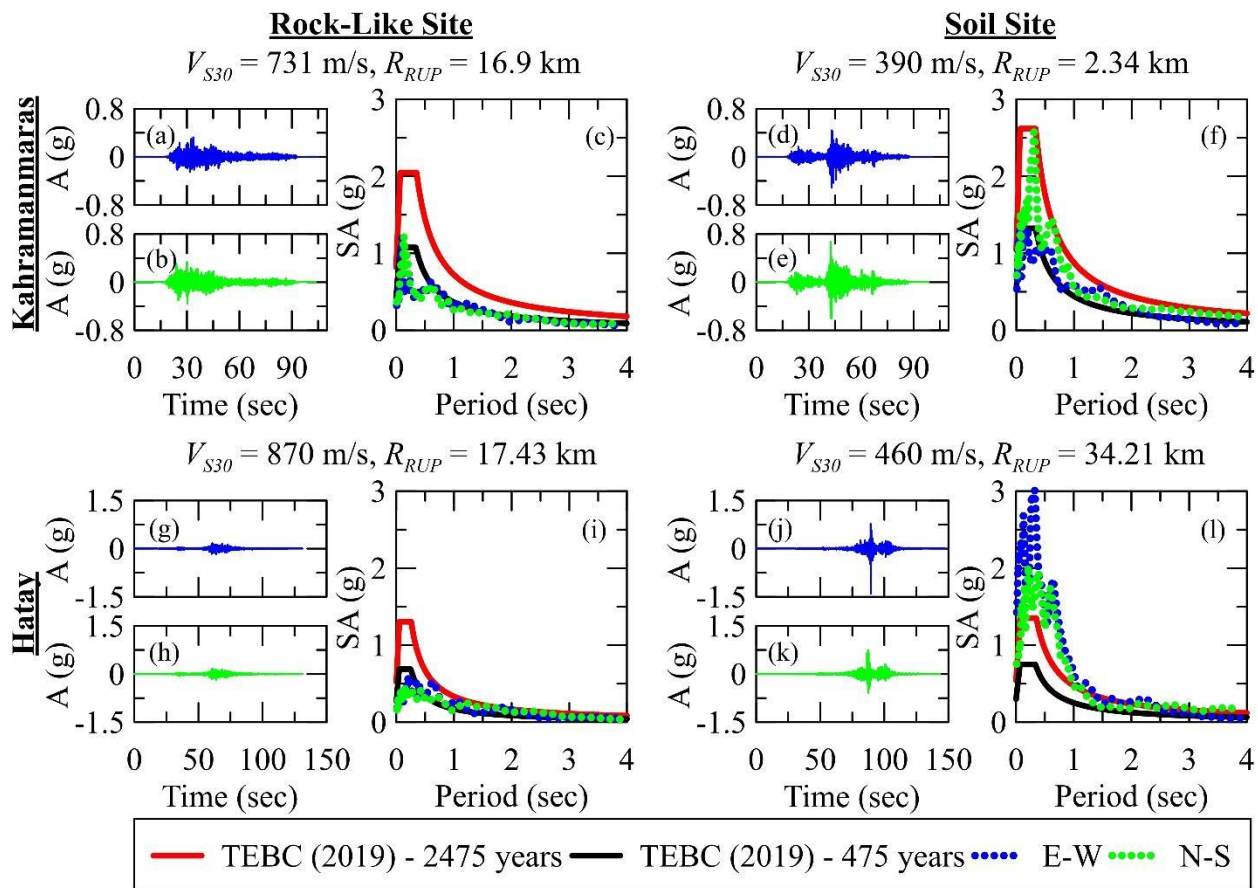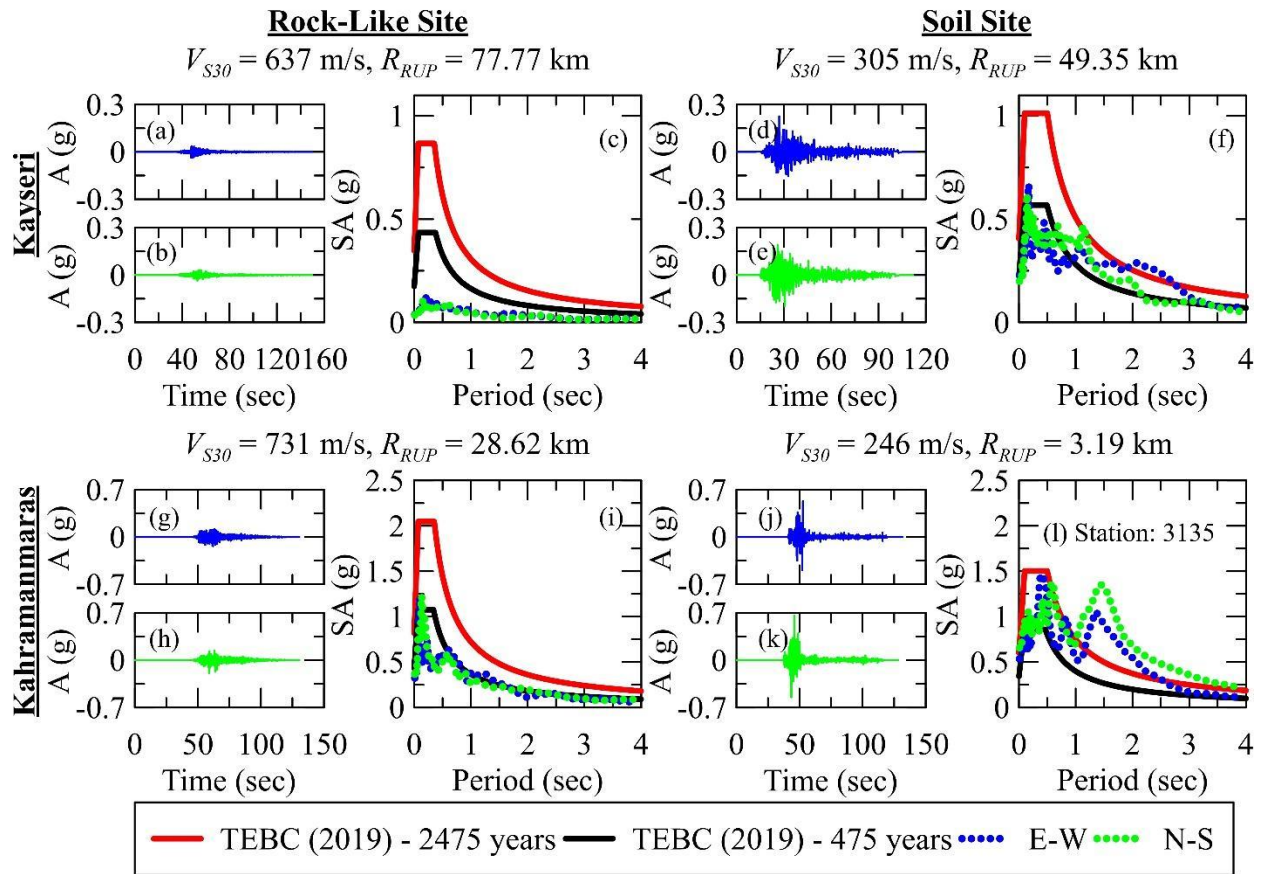
Figure 2-5 The baseline corrected acceleration (A) time histories in (a) E-W, (b) N-S directions, and (c) 5% damped response spectral accelerations (SA) and design spectra suggested by TEBC (2019) for return periods of 2475 years and 475 years for station ID of 3804 located in Kayseri. The same information is presented for (d, e, f) station ID of 3802, (g, h, i) station ID (Kahramanmaras) of 4611, and (j, k, l) station ID (Kahramanmaras) of 4612 (M$_w$ = 7.5 event).

2.4   Rupture Directivity Effects

The fault rupture that propagates towards the site is known to result in rupture directivity effects, which can be observed as a pulse-like behavior in the velocity time-history of the recorded strong ground motion that carries most of the seismic energy (Somerville et al., 1997). Such pulses can considerably influence the performance of upper structures under earthquake excitation such that (i) Anderson and Bertero (1987) stated that a structure located close to the near-field region might exhibit a dynamic response that is two times larger than a structure that is not exposed to near-field effects, and (ii) Alavi and Krawinkler (2000) indicates the occurrence of early yielding of the upper stories. Different methodologies have been developed to detect the pulses resulting from directivity effect (Hayden et al., 2014; Shahi and Baker, 2014), but this study identified pulse-like strong ground motions through visual inspection.
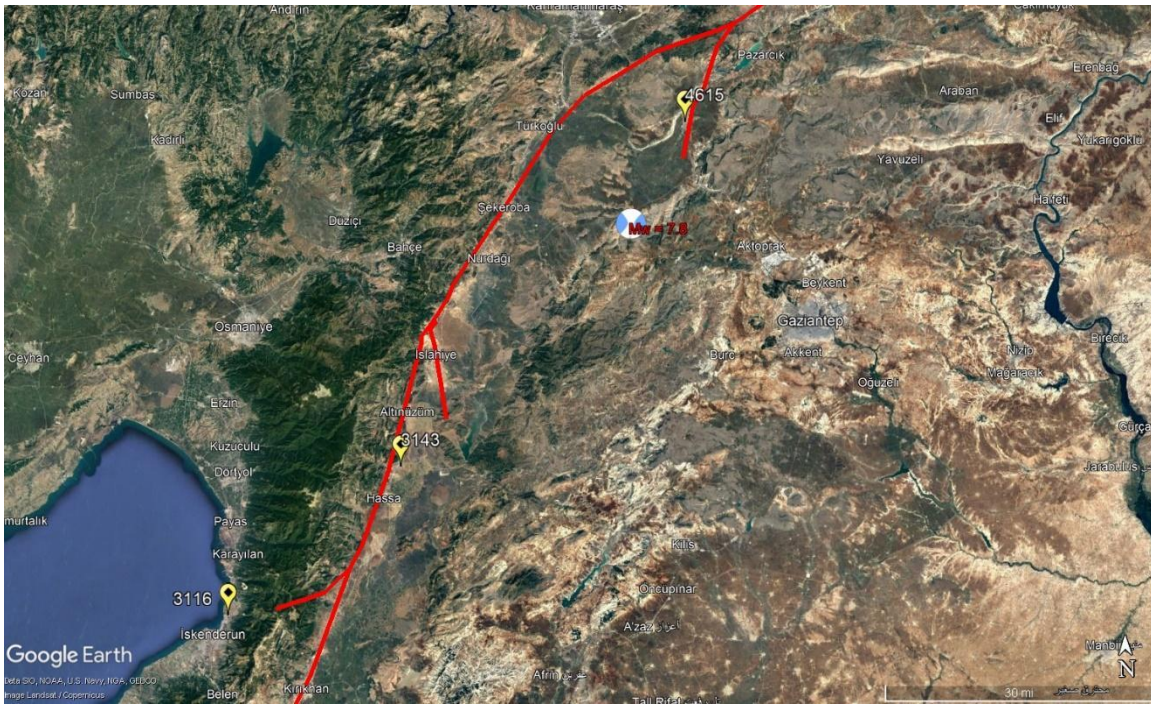
Figure 2-6 Station 3116, 3143 and 4615 along with the fault rupture in M_w 7.8 event.

Figure 2-6 exhibits Station 3116 with V_{S30} = 870 m/s and R_{RUP} of ~17.4 km in Hatay, Station 3143 with V_{S30} = 445 m/s and R_{RUP} of ~2.0 km in Hatay, and Station 4615 with V_{S30} = 484 m/s and R_{RUP} of ~0.9 km in Kahramanmaras along with the fault rupture for M_w 7.8 earthquake. All these stations with close distance to fault rupture are evaluated to be in forward directivity region, and thus the motions recorded in these stations during M_w 7.8 event are inspected for velocity pulses as presented in Figure 2-7 (Station 3116), Figure 2-8 (Station 3143), and Figure 2-9 (Station 4615). As a result, the significant velocity pulses in each record are observed in velocity time-histories as anticipated. Further investigation for detecting the velocity pulses in the motions recorded during M_w 7.8 and M_w 7.5 events is recommended to better understand the structural damages in the areas affected by the February 6th earthquakes.

Figure 2-7 The (a) acceleration and (b) velocity time histories, and (c) pseudo-spectral acceleration of Station 3116 (Hatay) for M_w 7.8 event.

Figure 2-8 The (a) acceleration and (b) velocity time histories, and (c) pseudo-spectral acceleration of Station 3143 (Hatay) for M_w 7.8 event.
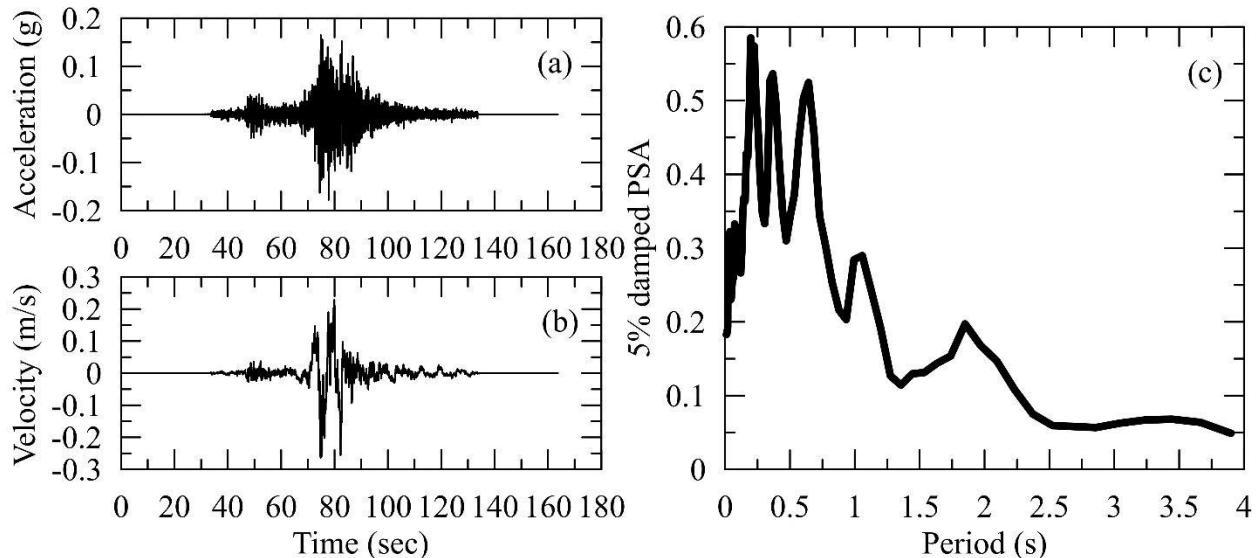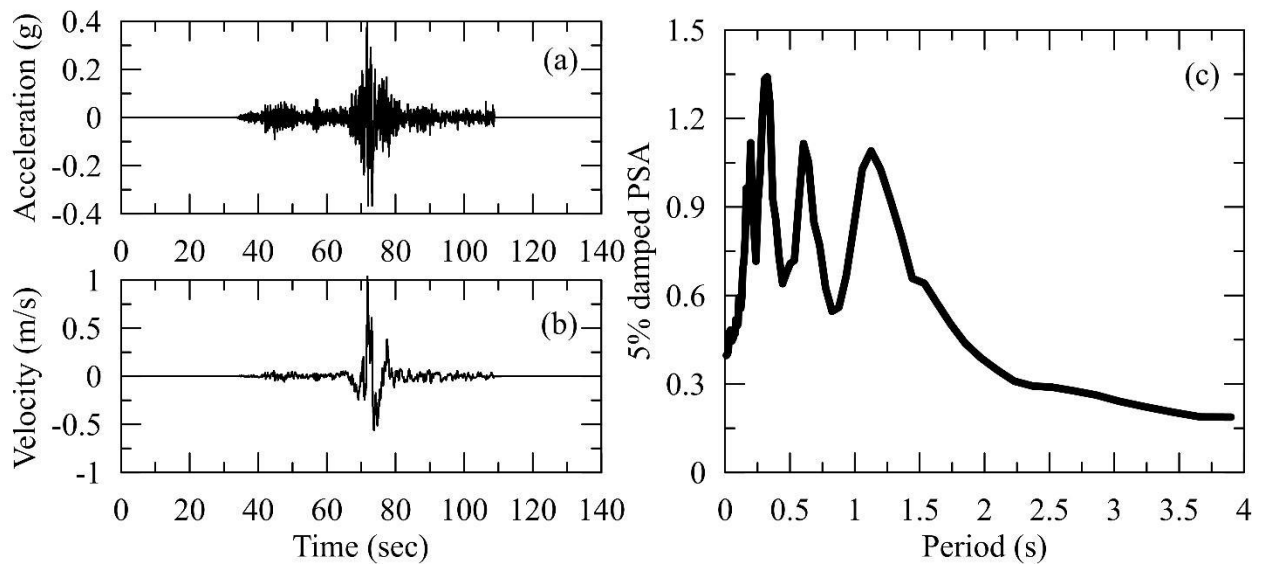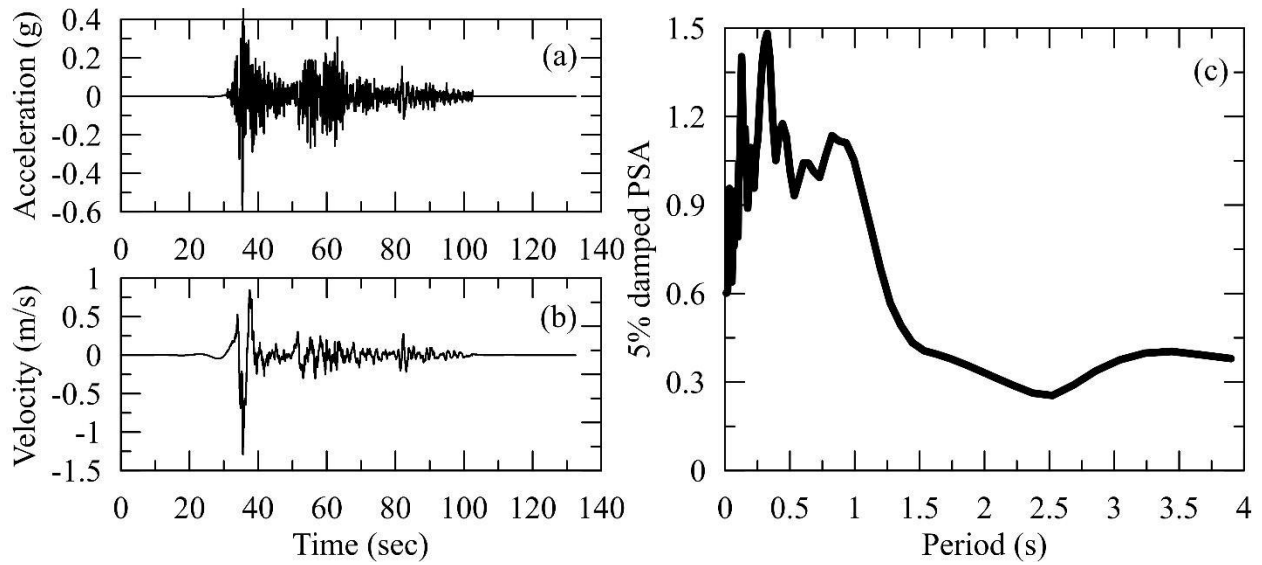

Figure 2-9 The (a) acceleration and (b) velocity time histories, and (c) pseudo-spectral acceleration of Station 4615 (Kahramanmaras) for M_w 7.8 event.

3 GEOTECHNICAL FINDINGS AND PERFORMANCE OF GEO-STRUCTURES

3.1 Overview

Moment magnitudes of 7.8 and 7.5 earthquakes struck Türkiye and Syria on February 6, 2023, within 9 hours. Two events and aftershocks impacted several provinces in the southeast of Türkiye. The geotechnical engineering team performed a reconnaissance mission to document geotechnical engineering related problems and collect perishable data pertaining to geostructures in the region immediately after the earthquakes. This chapter focuses on the preliminary investigations of the geotechnical aspects including earthquake-induced liquefaction manifestations, settlements, slope, and earth dam deformations and instabilities. An overview of the location where geo-tagged data (photo, measurement, drone footage) is given in Figure 3-1. Iskenderun experienced widespread liquefaction manifested with sand boils and ejecta on the surface. The settlements were observed both in near-free-field conditions and under the structures including the public dock of Iskenderun. Evidence of soil ejecta and significant settlements were observed around a multi-story building and a mosque built on a reclamation area. Settlements were between 5 and 30 cm under the multistory building, whereas settlements at the public dock reached 150 cm. The earthquakes triggered several landslides and dam deformations. The geotechnical engineering reconnaissance highlights the necessity of: 1) investigation for widespread liquefaction which occurred in Iskenderun; 2) monitoring of the earth dams, further identifying those damaged during the earthquakes and those that performed well; and 3) monitoring of the slope instability in Altinozu, Hatay.
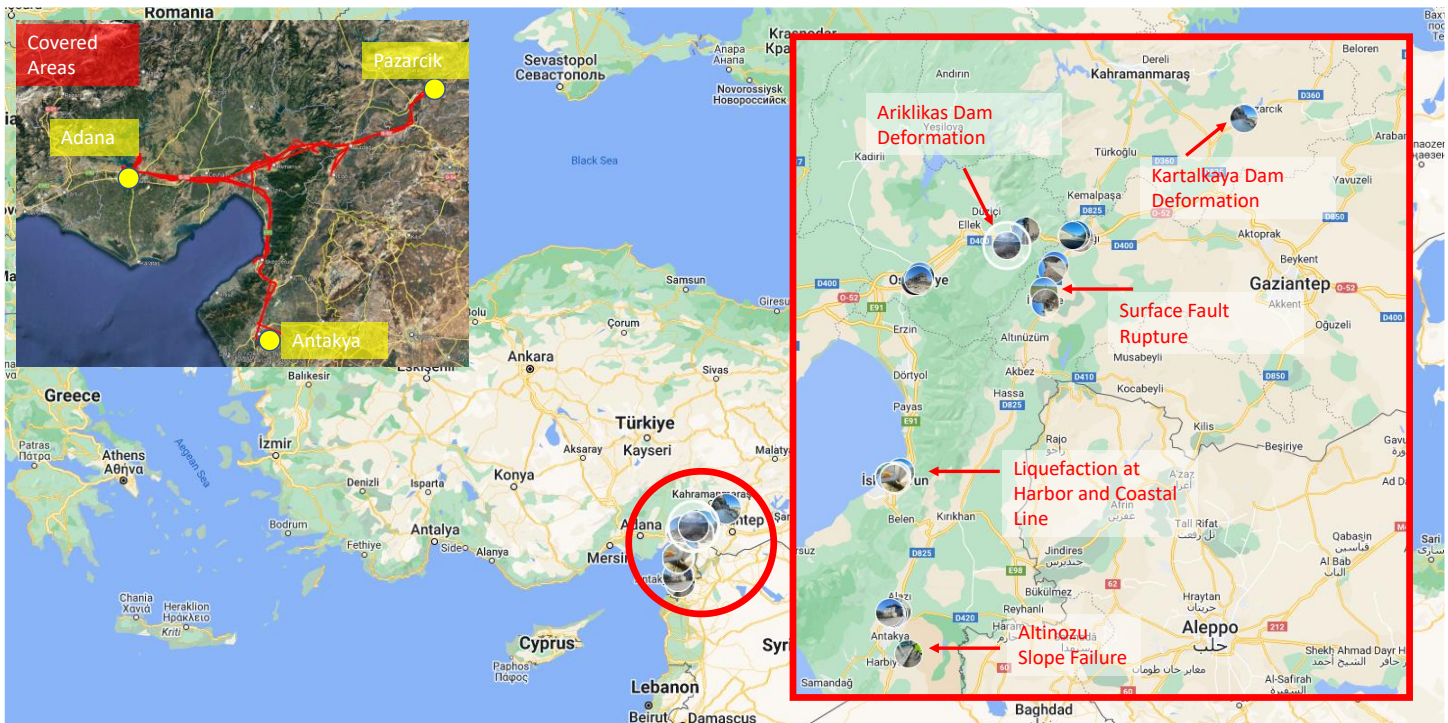
Figure 3-1 Plan-view of the geotechnical reconnaissance and covered areas

3.2 Seismic Soil Liquefaction

Iskenderun is nestled on the southern Mediterranean coast along the foothills of the Amanos mountains and stretches for about 5 kilometers. Coastal areas of Iskenderun are underlain by young marine deposits and artificial fill. There are also several creeks originating from the Amanos mountains towards the bay and these have contributed to the local soil formations. Young marine deposits and fills dominate the coastal plains covering part of the older sections of Iskenderun up until the town transitions into higher ground towards the foothills of the mountainous terrain. The soils along the coastal area include loose to medium dense sands and silty sands with variable thickness depending on the proximity to the coastline. Soil conditions are highly variable because of the marine and alluvial depositional environment as well as the reclamation fill. Most of the buildings are on shallow mat foundations and there are also high-rise structures on deep foundations and jet grout columns. Figure 3-2 through Figure 3-8 documents the

observations regarding liquefaction, liquefaction induced lateral spreading and ground deformations, and seismic deformations in different parts of Iskenderun. Preliminary observations indicate that Iskenderun experienced widespread liquefaction and lateral spreading. Sands and silty sands are prevalent within the area that suffered liquefaction-induced ground failure. Liquefaction was evidenced by ground cracks, sand boils, apparent subsidence, and lateral spread as well as the settlement of buildings on shallow foundations. It is estimated that the waterfront area settled by about 50-60 cm and the buildings on mat foundations in this area settled by about 5-50 cm. Ground subsidence as high as 150 cm was observed at the Iskenderun port situated at the northern end of Iskenderun. It was also observed that the severity and magnitude of liquefaction-related ground failure gradually diminished by about 400-500 meters inland from the waterfront. Buildings and structures founded on deep foundations and jet grout columns performed well without any catastrophic failure.
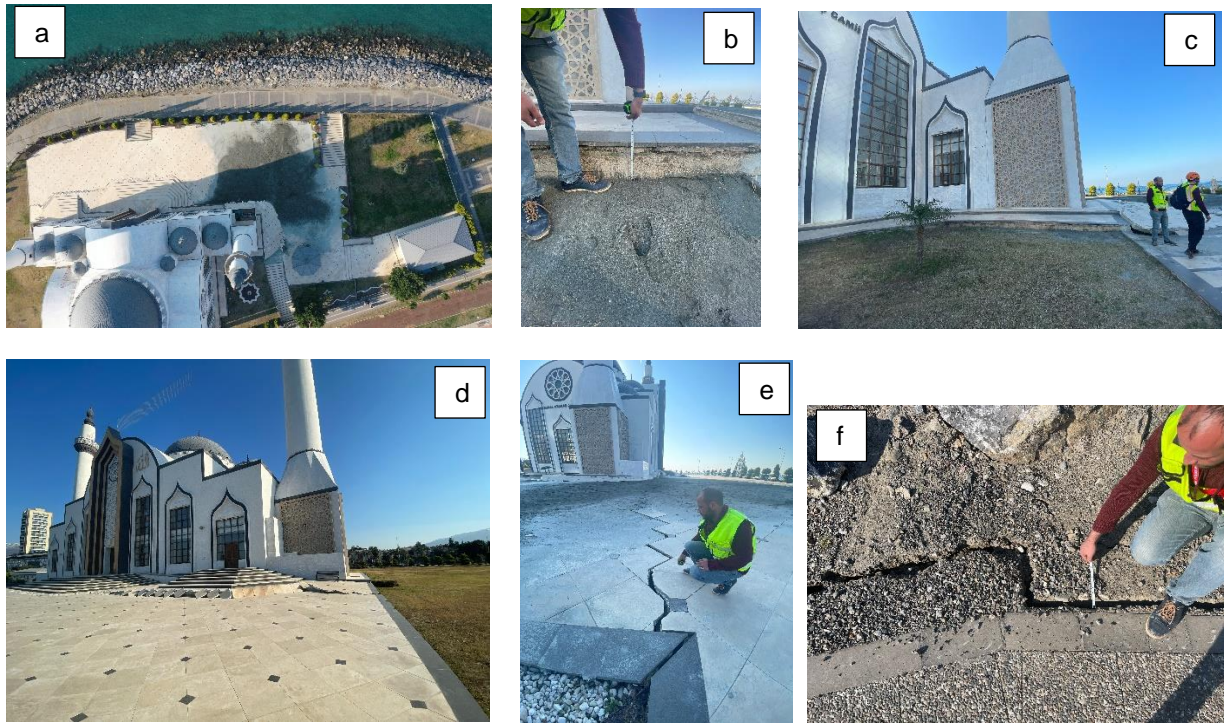
Figure 3-2 Liquefaction manifestations in Nihal Atakas Mosque (~ 36°35'35.27"N/ 36° 9'26.74"E): a) Bird's-eye view of the sand ejecta at the corner; b) settlements of the sand near the mosque; c) front view outlining the settlements; d) severe deformations observed on the marble ground due to liquefaction induced settlements; e) lateral spreading in front of the mosque; f)lateral spreading near the mosque towards the sea.

Figure 3-3 Liquefaction manifestations on Ataturk Boulevard near Forbes Shopping Center (~ 36°35'36.52"N/ 36° 9'34.67"E): a) sand boils on Ataturk Boulevard; b) cracks formed due to lateral deformation; c) cracks formed due to lateral deformation; d) liquefaction induced settlements; e) cracks formed due to lateral deformation.

Figure 3-4 Liquefaction manifestations (sand boils) on Ataturk Boulevard near Ataturk (~ 36°35'29.50"N/ 36° 10'20.23"E)

Figure 3-5 Liquefaction manifestations (sand boils) on Ataturk Boulevard (~ 36°35'26.86"N/ 36° 10'40.39"E)

Figure 3-6 Liquefaction manifestations on Ataturk Boulevard near Tennis Courts (~ 36°35'26.95"N/ 36° 10'28.39"E): a) water accumulation and sand boils; b) sand boils; c) ground settlement.

Figure 3-7 Liquefaction manifestation): a) Odeo Bank corner: sand ejecta and liquefaction induced settlements (~36°35'25.92"N/ 36° 10'25.46"E); b) Civilim building corner: sand ejecta (~ 36°35'23.48"N/ 36° 10'23.89"E).

Figure 3-8 Ground Settlements and Lateral Deformations on Iskenderun Dock (~ 36°35'40.67"N/ 36° 10'38.69"E): a) Ground subsidence at the pier and the lighthouse; b) Ground subsidence at the dock; c) Ground subsidence and lateral deformations of the concrete panels; d) lateral deformations and cracks on the concrete panel

3.3   Dams

Several earthquake-induced damages were observed at the Kartalkaya dam (Figure 3-9) in Kahramanmaras and Ariklikas dam in Osmaniye. The Kartalkaya dam has been supplying irrigation water to the Pazarcik County and tap water to the city of Gaziantep. The dam was built on the Aksu River for irrigation and for flood prevention for the town of Pazarcik. The Kartalkaya dam has a crest elevation of 720 m and catchment elevation ranging between 680 and 2,470 meters. It has been in operation since 1971 with a reservoir area of 11 km^2 and a drainage area of 1088 km^2 that can supply irrigation water to 200,000 acres of farmland. During the construction phase, the capacity was calculated as 200,000,000 m^3 but current capacity has decreased to 160,000,000 m^3 because of the sediment fill in the reservoir. The sediment fill caused by the rainfall-induced erosion has led to the several studies focusing on erosion in the area (Yuksel et al., 2008; Taskesen Ozturk, 2018).

The reconnaissance team documented significant damage on the crest and right wing of the Kartalkaya dam. The damage is associated with the combined effect of seismic load-induced cracks and lateral displacements at the central part of the crest, and rockfalls on the upstream part of the dam. The cracks are longitudinal to the dam crest, reaching values of twenty meters long and having a depth of 0.5 m and a width of 0.3 m. No significant orthogonal cracks were observed in the crest. There was no upstream or downstream damage observed at the side slopes. The reservoir has already been almost empty due to the present climate, and there was no leakage through the gates. Wings located at the water inlet through the gates have damage due to the intense shaking. One segment moved toward the earth dam, where seismic compression occurred. There are no connections between segments on the wings so that damaged segments easily move apart.

(a)

(b)

(c)
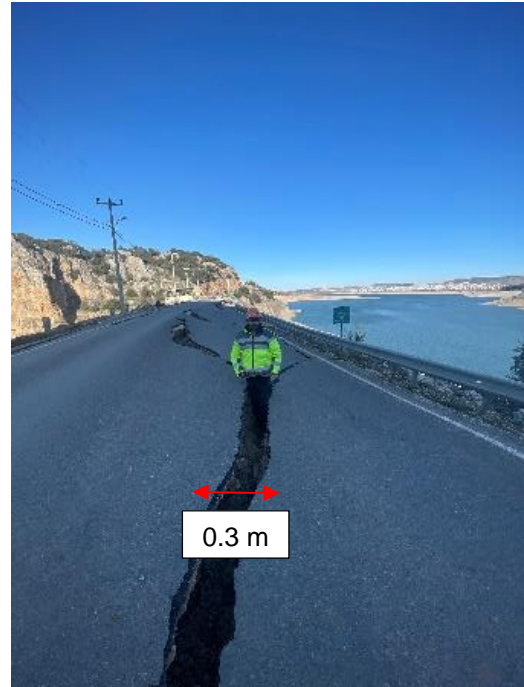
(d)

Figure 3-9 Deformations observed on the Kartalkaya dam (~37°28'06.01"N/ 37°14'20.14"E): (a) Compression cracks and lateral displacements at the crest of Kartalkaya dam ; (b) moved segment and compression; c) earthquake-induced rock fall and associated cracks on the crest; (d) Longitudinal cracks in the middle of the crest

The Arıklıkaş Dam is a homogenous earth-fill dam constructed between 1994-1998 in Osmaniye for irrigation purposes. The crest height from the stream level is almost 32 meters. Cracks were formed during the earthquakes at the crest level, and the crack widths range between 2.2 m and 4 m. Lateral movement is toward the upstream, and no damage was detected on hydraulic structures except for minor cracks on the curtain walls of the spillway. In addition, the face of the dam at the upstream side was observed to be significantly settled close to the crest and bulged out towards the toe of the dam with a visible opening at the center of the slope (see Figure 3-10 for the photos).
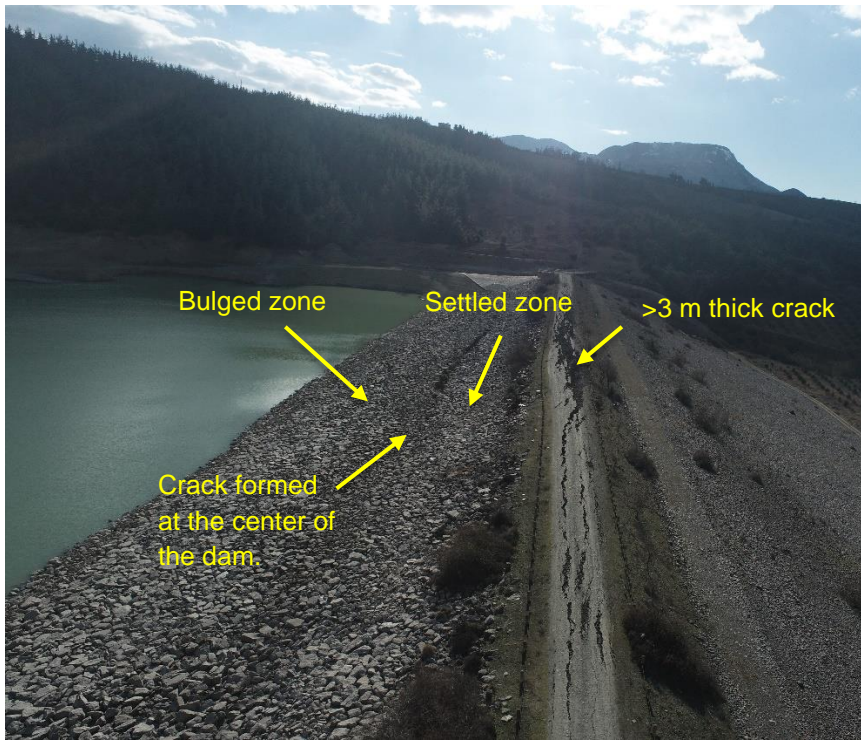
(a)   (b)

Figure 3-10 Deformations observed on the Ariklikas (~37°09'25.70"N/ 36°30'55.96"E) dams: a) Ariklikas Dam (side view); b) Ariklikas dam construction details (in Turkish)

The Yarseli Dam is an earth-fill dam constructed between 1985-1991 in Antakya for irrigation purposes. The crest height from the stream level is almost 37 meters [Figure 3-11(a)]. Crest cracking with lateral displacements vary between 0.15-0.25 m, as can be seen in Figure 3-11(b). There were no sand boils on the earth-dam surface, so no trace of liquefaction was found. The hydraulic structures had no obvious cracking or damage.

(a)   (b)

Figure 3-11 Arial pictures of the Yarseli dam (36.194290N, 36.329264E): (a) Overview; (b) Cracks in the crest

3.4   Test Center

Tepehan village near Altinozu, Hatay experienced a large-scale slope instability after the earthquake sequence. Arial footage taken in the area shows the canyon-like terrain after the earthquake created very large cracks having dimensions of 300m x 200m x 30m. The geology of the area was investigated by Selcuk (1985), and it reveals a Middle Miocene aged Tepehan formation, which consists of sandstone, clayey limestone, claystone, and marl. Sandstones are usually medium-thick bedded loosely packed and contains significant amount of thin fossil shells that are prone to breakage.

The slope angle ranges from 10 to 30 degrees. The area had been particularly dry for several years, but there was a heavy rainfall that lasted for several days preceding the earthquakes, inundating and saturating the soil. Figure 3-12 presents aerial photos taken at the slope instability area.

Figure 3-12 Landslide at an olive farm near Türkiye-Syria border (Altinozu, Hatay): a) main crack (bird's-eye view) at ~ 36°09'42.41"N/ 36°13'13.40"E; b) main crack – near-front view of the crack; c) and d) 2 meter crack formed several hundreds of meters away from the main crack at ~ 36°09'28.18"N/ 36°13'00.65"E

Another landslide was documented in the Fevzipaşa-Meydanekbez segment running N-S from the main Adana-Gaziantep rail line towards Aleppo, Syria. The approximate location of the landslide is marked in Figure 3-13. As can be seen in the map, this a very critical location because it is one of the few segments connecting Syria with Türkiye.
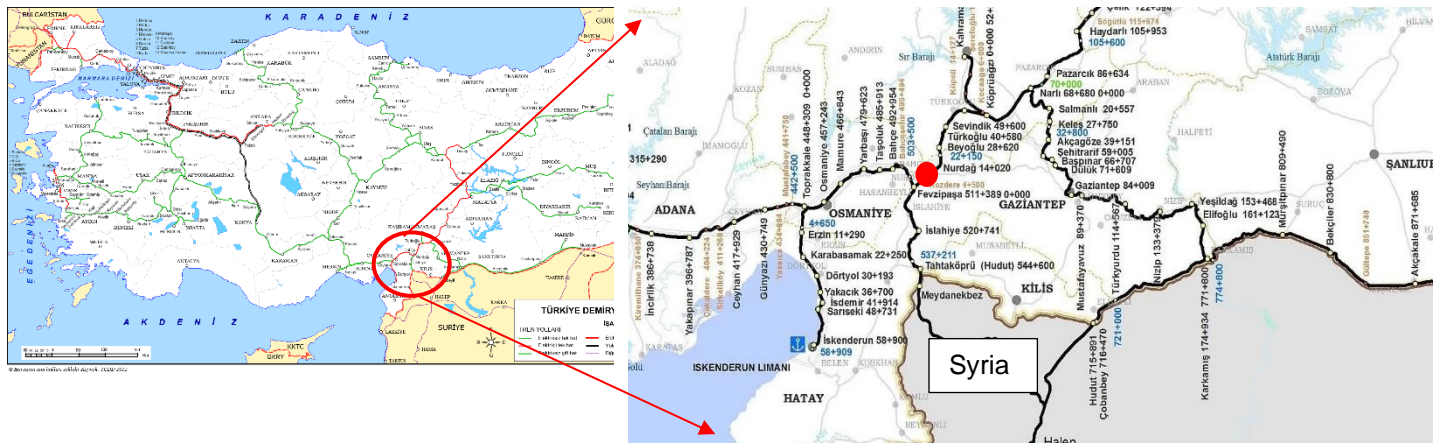
Figure 3-13 Overview map of the railroad map of Türkiye-Syria and landslide location (~ 37°06'43.41"N/ 36° 39'34.91"E)

The collected data is not enough to report if the landslide was caused by the first or second earthquake in the sequence. Arial footage of the landslide indicates that the head scarp is approximately 100 meters long. Several backhoes were immediately sent to the site for debris removal.
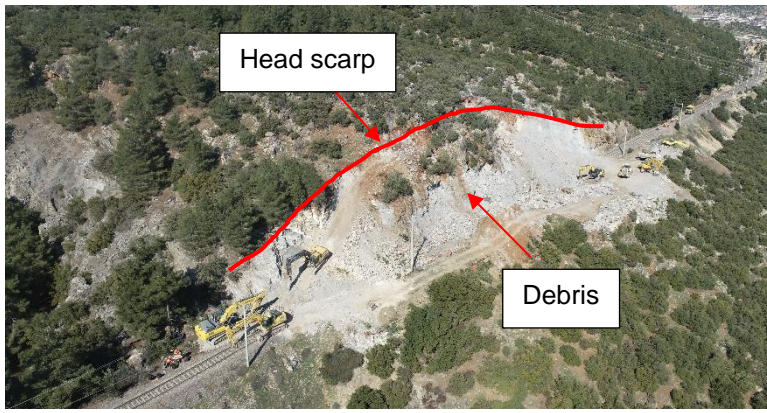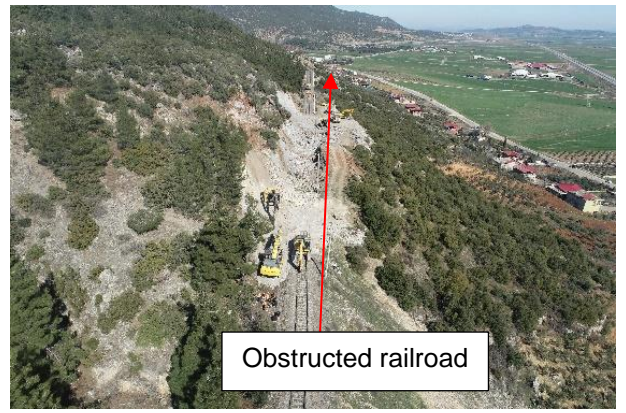
(a)   (b)

Figure 3-14 Landslide near a railroad in Islahiye at ~ 37°06'43.41"N/ 36° 39'34.91"E (arial photos taken for the same slope failure at different angles)

4 PERFORMANCE OF RESIDENTIAL STRUCTURES

4.1 Overview

The structural reconnaissance team visited the region affected by the earthquake sequence on March 20, i.e., two weeks after the earthquakes. It was observed that demolition work had started before the reconnaissance [see Figure 4-1(a)], i.e., some heavy machines, such as excavators with buckets or claws, had pulled down some damaged buildings, as shown in Figure 4-1(b). An effort was made to exclude the damage states of buildings that were possibly exacerbated by demolition work [e.g., Figure 4-1(c)] as noted by discussion from local authorities. Overall, the observations were in agreement with reported condition assessments conducted by the Ministry of Environment and Urbanization of Türkiye (MEUT) on 736,851 buildings in the effected region. Collected data shows that a total of 19,284 buildings collapsed from the earthquake sequence and almost half of the investigated buildings (373,038) were damaged to varying levels, as shown in Table 1.

Table 1 Structural damage levels in cities by percentage (%) (MEUT Report, 2023)

City	Damage Level					
	None	Slightly	Others	Extensive	Partial Collapse	Full collapse
Adana	72.11	21.71	5.51	0.51	0.05	0.12
Adiyaman	29.9	32.54	14.58	15.9	1.85	5.23
Diyarbakir	59.79	24.2	13.55	1.85	0.14	0.47
Gaziantep	59.7	18.27	15.42	4.35	0.71	1.55
Hatay	49.47	23.54	7	13.36	2.31	4.32
Kahramanmaras	37.75	28.69	14.75	12.43	2.66	3.72
Kilis	50.39	31.39	9.31	5.83	0.78	2.29
Malatya	26.12	26.89	20.65	21.57	0.63	4.13
Osmaniye	63.98	20.98	8.34	5.66	0.58	0.46
Sanliurfa	49	34.85	15.16	0.78	0.09	1.3

| (a) | (b) | (c) |

Figure 4-1 (a) Demolishing work, (b) an excavator pulled down the damaged buildings, (c) the damage states of buildings possibly contaminated by demolishing work.

4.2 Reinforced Concrete (RC) Buildings

4.2.1 Construction and Materials

Figure 4-2(a) and (b) reveal two different construction practices in Türkiye. By observing the forms and scaffolding, Figure 4-2(a) indicates that the fresh concrete of columns, beams, and slabs of a story was cast as a whole. In contrast, Figure 4-2(b) indicates that the fresh concrete of columns was cast first and then followed by casting the fresh concrete for beams and slabs. The integrity of the building using the former approach [see Figure 4-2(a)] should outperform that of the latter [Figure 4-2(b)]. Moreover, Figure 4-2(c) shows an existing two-story building with an additional third story. Because the dead load of the building was amplified approximately 1.5 times, it would have certainly increased the seismic risk of that building if the existing two stories were not adequately strengthened. Figure 4-2(d) shows that instead of deformed

rebar, plain reinforcement was used and, as a result, bond between rebar and concrete was poor. In addition, the spacing of stirrups was large at approximately 30 to 40 cm, with coarse aggregates seeming to be too small [Figure 4-2(d)] since these buildings were designed by using the old seismic code. Figure 4-2(e) and (f) show that there is no separation between buildings. In other words, seismic damage resulting from pounding between buildings likely occurred.

Figure 4-2 (a) and (b) two buildings with different construction practices, (c) a building with an added third story, (d) poor concrete and plain reinforcement, (e) and (f) no separation between buildings.

4.2.2 Collapsed Buildings

In terms of the appearance of building collapse, it is straightforward to categorize them into "lie-down", "sit-down", and "knee-down" types (Lin et al. 2020). The occupants of lie-down collapsed buildings have almost no chance of survival, which usually causes the most fatalities during seismic events. The sit-down and knee-down collapsed buildings only directly threaten the lives of occupants of fully or partially collapsed stories, rather than all stories. Figure 4-3(a) and (b) are lie-down collapsed buildings, one of which was still under construction, with its sale advertisement nearby [see Figure 4-3(a)], while the other building was occupied, as shown in Figure 4-3(b). If the lateral force-resisting system of the building shown in Figure 4-3(a) had been completed before the earthquake, the soft-and-weak lower story of the building could be attributed to either design or construction issues, rather than the possibility of the building being remodeled by occupants. Figure 4-3(c) is a sit-down collapsed six-story building with a pancaked third story which is also called a soft story. Figure 4-3(d) shows three similar eight-story buildings with different damage levels. The left building partially pancaked at the second, third, and top stories [see Figure 4-3(e)], but the other two buildings were only moderately damaged. This observation implies that the lateral force-resisting elements on the front side of the second and/or third stories of the left building probably had been remodeled before the earthquake, which resulted in the weak second and/or third stories.

The far-right building in Figure 4-3(d) has a masonry wall at the first story so its damage was less than that observed in the mid building. The wall showed shear failure with two major diagonal cracks at angles of 45° and 60° [Figure 4-3(f)]. Additionally, bi-directional and one-directional plastic hinges were successfully formed at the bottom ends of the first story columns [Figure 4-3(g)]. The bi-directional plastic hinge indicates that the building suffered significant ground motion in both mutually perpendicular horizontal directions. Because strength deterioration of a column in one direction affects the performance of the column in the other direction, three-dimensional analysis and design of buildings should be stressed in the future. Figure 4-3(h) and (i) show a knee-down collapsed building, in which the beams were separated from the columns and walls. By observing the almost intact surface of the beam bottom, it indicates that the beams were inadequately connected not only with the walls, but also with the columns. Furthermore, by observing the relatively separated locations between the beams and columns of the first story, this building was likely displaced rightward and inward of the photograph.

Figure 4-3 (a) and (b) lie-down collapsed buildings, (c) a building with pancaked third story, (d) and (e) three similar buildings with different damage states, (f) close-up photograph of the first story of the right building, (g) bi-directional and one-directional plastic hinges, (h) and (i) a knee-down collapsed building.

That is to say, the building experienced rotational displacement demands in plan view (twisting) under the earthquake. Some buildings collapsed or were damaged by issues (e.g., soil liquefaction) other than structural. Figure 4-4(a) and (b) illustrate an overturned building and unequal settlement of a building, both with good structural integrity. Figure 4-4(c) and (d) show ground settlement, surface cracking, and sand boils, which indicate soil liquefaction in that area. Secondary disaster caused by the earthquake was also noticed; Figure 4-4(e) shows a building, in which damage caused by fire is perhaps more serious than that caused by the earthquake shaking. Figure 4-4(f) indicates a slightly-to-moderately damaged five-story building with some damaged facilities (e.g., water tanks) at the top of the roof. Although the building was successful against the seismic strike, damage of nonstructural components certainly affected the function of the building.

4.2.3 Structural Members

Figure 4-5(a) and (b) show that two buildings collapsed along the street because the weak direction of columns was oriented along the street. The large aspect ratio of column cross-sections, rather than a square, seems to be common in the region that was observed to increase indoor space. Nevertheless, once all columns are oriented in the same way, the building would be soft and weak in the weak-axis direction of the column, i.e., the vulnerable direction of the building to earthquakes. In addition, the strong beam-weak column concept likely exists in the weak direction [i.e., plastic hinges will be formed in columns rather than in the beams, such as that shown in Figure 4-5(c)]. Figure 4-5(d) shows the weak-direction plastic hinges at the bottom ends of the columns. Additionally, the spacing of stirrups within the plastic hinge zones was greater than 20 cm. Figure 4-5(e) and (f) show an almost intact five-story building. The close-up photograph of the first story indicates that the orientation of columns is not the same (i.e., some columns are rotated 90° in relation to the other columns). Note that while arranging the orientation of columns with large aspect ratios, not only the overall stiffness of columns in each horizontal direction, but also the plan distribution of columns, should be carefully considered. Otherwise, buildings are possibly plan-asymmetric, i.e., they will simultaneously translate and rotate in plan view from ground motions.

Figure 4-4 (a) An overturned building, (b) unequal settlement of a building, (c) settlement of ground, (d) sand boils, (e) secondary disaster, (f) damaged facilities atop a roof.

Figure 4-6(a) shows two buildings at one construction project. The progress of the right building was ahead of that of the left building. Figure 4-6(a) shows that the exterior and partition walls (often called infill walls) are usually made of bricks, which are erected after completing the beam-column frame system. The thickness of typical brick walls is 15 cm, which consists of 10 cm thickness of bricks and 2.5 cm covering on both sides of the bricks [see Figure 4-6(b)]. Because there are no connectors between the brick walls and beams/columns, the brick walls fall out of the beam-column frames [see Figure 4-6(c) to (e)]. At this point it is not clear if the infill walls are considered in the structural analysis and design of the buildings in Türkiye. Nevertheless, Figure 4-6(f) shows that the infill walls indeed share the seismic force and partially support the building weight. Beams and columns were thus protected from damage to a certain extent [Figure 4-6(f)]. However, the participation of infill walls in the lateral force resistance significantly increases the lateral stiffness of beam-column frames. Therefore, the actual vibration periods of buildings with infill walls are substantially less than those obtained from numerical models without considering infill walls. In other words, the actual sustained seismic force of buildings is probably greater than the design base shear obtained from the numerical models without considering infill walls. Also infill walls falling to the streets represents a severe hazard to people. Türkiye should decide to either consider infill walls in the seismic performance or not. These walls should be connected properly to the RC frame members and bricks or blocks properly connected to each other. If the infill walls are not to be considered for seismic resistance, gaps should be provided between the walls and frame members.

The floor slab systems used in Türkiye seem to be categorized into two types: one type is supported by beams and columns [see Figure 4-7(a)] and the other type is supported by only columns which can be called hidden beam slabs [i.e., no beams, as shown in Figure 4-7(b)]. The hidden beam slab usually consists of a flat slab that is reinforced with steel bars and has a shallow beam integrated into it. The beam is usually placed at the perimeter of the slab and is surrounded by the concrete slab. The beam and slab work together to transfer loads from the structure above to the supporting columns or walls. However, it was observed that these slabs are made of bricks, whereas the bricks are possibly fallen down from earthquakes, as shown in Figure 4-7(c) and (d). In light of some collapsed or seriously damaged buildings consisting of that floor slab system [e.g., Figure 4-7(b) and Figure 4-7(e)], which is a close-up photograph of the left building shown in Figure 4-7(c)], the seismic performance of the no-beam slab system is certainly in doubt.

Figure 4-5 Structural damages (a) and (b) collapsed buildings along a significantly weak direction; (c) plastic hinges at top and (d) plastic hinges at bottom of columns, (e) an almost intact building, and (f) a close-up photograph of (e).

Figure 4-6 (a) Two buildings of one construction project, (b) a typical brick, (c) and (d) brick walls popped out of frames, (e) brick walls fallen down, (f) beams and columns were almost intact but brick walls seriously cracked
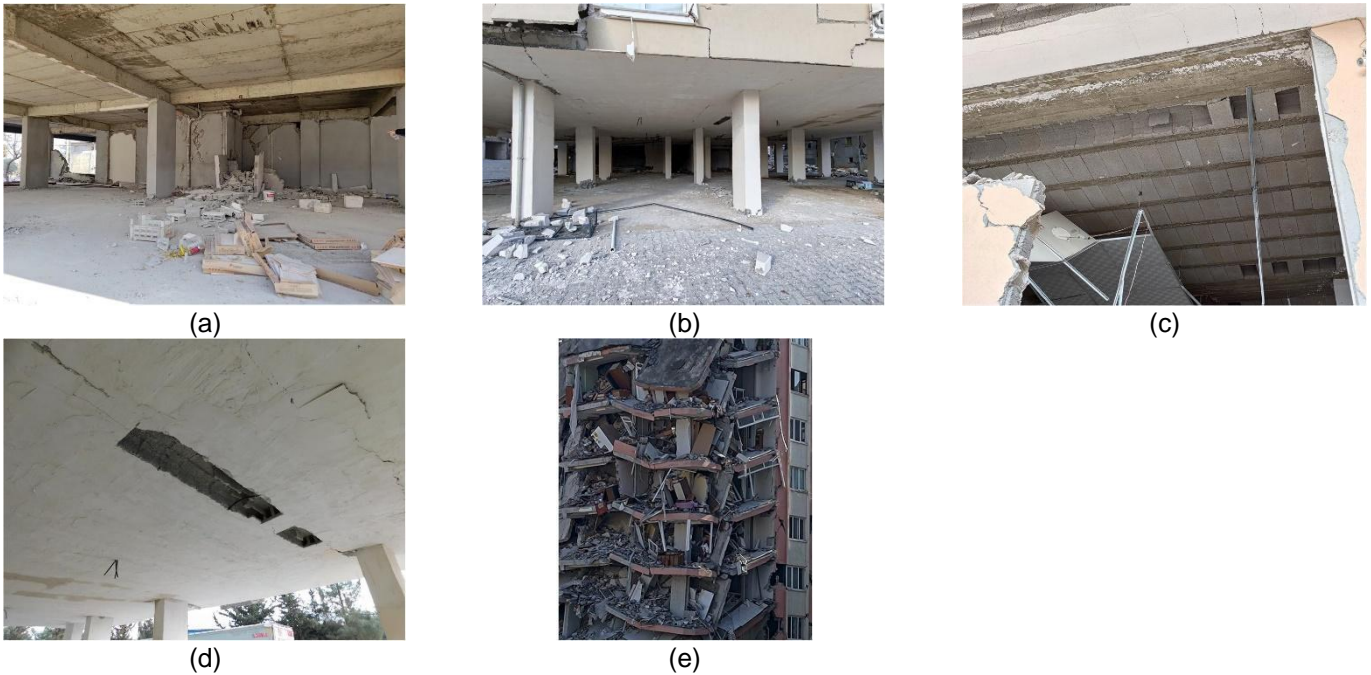
(a)

(b)

(c)

(d)

(e)

Figure 4-7 A floor slab system (a) supported by beams and columns, (b) directly supported by columns, (c) and (d) bricks of the no-beam slab system fallen down, (e) a building with the no-beam slab system was under demolition.

In Türkiye, close and open overhangs are commonly used in building design, such as balconies, semi-balconies, and extended rooms. However, previous earthquakes have shown that buildings with overhangs tend to sustain more damage compared to those without. Despite that the Turkish seismic design code allows for overhangs and requires them to be designed to withstand seismic loads, numerous issues during construction have been reported in post-earthquake assessments (GEER 2020, DAUM 2020, METU-EERC, 2011). Damage examples caused by overhanging structures are shown in Figure 4-8(a) and (b). High stress is placed on the columns at cantilever beam connections that intersect with overhangs, leading to significant structural damage at these critical locations. To increase rigidity at these junctions, it may be advisable to use reinforced concrete walls instead of columns if overhangs are unavoidable. A common type of column damage occurs when the columns are partially restricted from lateral movement by strong infill walls or non-structural partitions of partial heights. These captive columns are prevalent in many buildings, often found in areas such as staircases, toilets, and rooms with windows, primarily because structural engineers do not typically consider them in their earthquake-resistant designs. As shown in Figure 4-8(c), these captive columns can sustain significant damage during earthquakes. Additionally, it has been demonstrated that equations provided in the main design codes, such as ACI 318, cannot accurately predict their shear capacity, with the difference sometimes exceeding 150%. Consequently, their existence in buildings should be avoided.

(a)

(b)

(c)

Figure 4-8 Residential building damages (a) due to overhangs, (b) captive/short column due to strong infill walls

4.3   Reinforced Concrete (RC) Buildings

Masonry buildings were generally located in rural areas of the seismic disaster regions. Figure 4-9(a) and (b) show that two old masonry buildings made of clay bricks were essentially intact, or slightly damaged, despite the two buildings seeming to be not engineered structures. The masonry walls and tiled roof stayed with structural integrity from the earthquake. Note that the water tanks atop the roofs remained, i.e., no damage to the supports of the water tanks. Because one-story masonry buildings are very stiff, ground accelerations are not amplified much at the roof line. In contrast, some similar water tanks on top of mid-rise and low-rise buildings in urban areas were toppled down [e.g., Figure 4-4(f)]. This observation means that whether the supports of water tanks are strong enough depends on the roof acceleration demands, which are usually greater as the number of stories increases. Figure 4-9(c) shows a relatively new stone masonry structure, which also seemed to be intact from the earthquake. Figure 4-9(d) and (e) show moderately damaged masonry buildings with a few fallen bricks and diagonal shear crack on the wall. Figure 4-9(f) and (g) illustrate severely damaged masonry buildings with crushed or toppled brick walls at the corners. This observation indicates that brick walls subjected to bi-directional forces are a specific vulnerability of masonry buildings. Lack of connection between orthogonal walls in masonry structures may cause damage if these walls do not share some bricks to act together; as shown in Figure 4-9(f) was made of two-leaf brick walls. In light of the different damaged heights between the two leaves of brick walls, the mortar between the multi-leaf brick walls seemed to be insufficient. Figure 4-9(h) shows that the entire gable wall of a masonry building almost disappeared, which probably had been cleared away after the gable wall toppled. In addition, the roofs adopted in the buildings shown in Figure 4-9(f) to (h) seemed to be simply rested on top of perimeter walls. Therefore, the roofs had no capacity to constrain the out-of-plan collapse of the walls. Figure 4-9(i) illustrates that a pure sliding mode failure mechanism of a brick wall occurred at a one-story masonry building, which probably resulted from the thrust of the next three-story building.

(a)	(b)	(c)
(d)	(e)	(f)
(g)	(h)	(i)

Figure 4-9 (a) to (c) essentially intact or slightly damaged masonry buildings, (d) and (e) moderately damaged masonry buildings, (f) to (h) severely damaged masonry buildings, (i) a pure sliding mode of failure mechanism of a brick wall.

4.4   Steel Buildings

Only one steel building was observed during the six-day structural seismic reconnaissance [see Figure 4-10(a)]. Entry into that steel building, which is a new museum with exterior circular columns and box girders [Figure 4-10(b) and (c)], was not permitted. Therefore, the state of the interior structure is unknown. Once the spectral value of the experienced ground motion at the fundamental vibration period of the building surpassed the corresponding design spectral value, some damage (even minor yielding) would be expected. Nevertheless, the building seemed almost perfect (elastic) in terms of its appearance from the outside, as shown in Figure 4-10(a). It is thus reasonable to infer that either the spectral value did not surpass the design spectral value, or some energy dissipation devices (or base isolators) were deployed in the building.
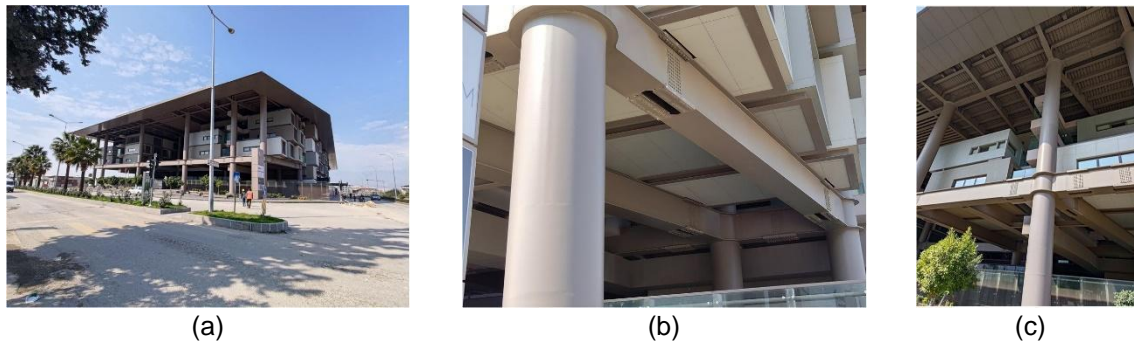

| (a) | (b) | (c) |

Figure 4-10 (a) A steel building, (b) splices of beam segments, (c) a beam-column joint.

4.5   Seismic Demands of Buildings

In light of the reconnaissance results, the factors of structural deficiencies are multiple, which are caused from issues of material properties, design, construction, and possible building remodeling by occupants. Besides the aspect of structural capacity, the seismic demand of buildings under the Türkiye earthquake is worth exploring. Figure 2-4 indicates that the seismic demands of some low-rise buildings in Hatay are significantly beyond the design spectral values with a 2475-year return period. In addition, Figure 2-5 indicates that the seismic demands of some mid and high-rise buildings in Kahramanmaras substantially surpass the design spectral values with a 2475-year return period. Therefore, considering the observed structural deficiencies, severe damage and even collapse of some buildings in the two cities are predictable. Moreover, in terms of damage accumulation, it is quite a challenge of the seismic resistance of buildings that sustained an earthquake of magnitude M_w 7.8 followed by another earthquake of magnitude M_w 7.5, not to mention numerous aftershocks. The effect of accumulative damage on the fragility curves of buildings is worthy of further study and to be reflected in future seismic design codes.

Figure 2-9 shows a near-fault pulse-like ground motion record with the peak ground velocity (PGV) approximately equal to 130 cm/s [Figure 2-9(b)]. The corresponding pseudo-spectral acceleration (PSA) spectrum [Figure 2-9(c)] indicates that the plateau of the PSA spectrum extends to approximately 1 sec, which is much wider than those of design response spectra illustrated in Figure 2-4(c), (f), (i), (l) and Figure 2-5(c), (f), (i), (l). In addition, most of the spectral values at long periods (up to 4 sec.) are greater than 0.3 g [Figure 2-9(c)], which is greater than the design spectral values illustrated in Figure 2-4 (c), (f), (i), (l) and Figure 2-5(c), (f), (i), (l). Note that the design PSA spectra shown in Figure 2-4 and Figure 2-5 are those without considering near-fault (NF) modification factors. In other words, in comparison with far-field ground motions, NF pulse-like ground motions likely result in PSA spectra with wider plateaus and greater spectral values at long periods. Kalkan and Kunnath (2006) questioned the validity of the process of amplifying elastic design spectra with NF factors to reflect NF effects, which is commonly stipulated in design codes. That study concluded that acceleration and velocity response spectra should be collectively examined to rationally assess the damage potential of NF ground motions. Considering that pulse-like ground motions generally infuse substantial energy into structures within a rather short period of time, Lin (2022) proposed power demand as a measure that reflects the threat of pulse-like ground motions to buildings. The role of near-fault pulse-like ground motions in the seismic damage of buildings from the Türkiye earthquake sequence certainly deserves further examination.

5 PERFORMACE OF BRIDGES

5.1 Overview

It is significant that tens of thousands of buildings collapsed in southern Türkiye from the sequential M_w 7.8 and M_w 7.5 earthquake events and, as far as the team knows, not a single bridge structure collapsed, although some were heavily damaged, which is expected and designed for in such a large event. Bridge structures have collapsed from smaller earthquakes in California than those just experienced in southern Türkiye, such as from the M_w 6.6 1971 San Fernando earthquake (USGS, 2021), M_w 6.9 1989 Loma Prieta earthquake (Governor's Board, 1989), and the M_w 6.7 1994 Northridge earthquake (DoT, 1994). In some instances, the bridge structures that failed in past California earthquakes were over 100 miles (161 km) from the epicenter. Perhaps bridges did not collapse in southern Türkiye because Türkiye has been keeping up with the most recent seismic bridge design specifications from California (Caltrans, 2019), and elsewhere, that improve from lessons learned after each major earthquake.

This revelation that no bridges collapsed from the earthquake sequence in southern Türkiye was from (1) the team's own observations of more than 10 bridges that were inspected, as well as ones that were driven past and over while traveling from town-to-town in the affected areas of southern Türkiye, and (2) multiple meetings and discussions with Turkish professionals and people living in Türkiye. It is probable that this is because buildings are typically private ventures while bridges are state sponsored. Thus, bridges were, for the most part, designed and built to modern specifications for earthquake response while buildings often were not, even though current Turkish building seismic design specifications (TEBC, 2019) are essentially identical to US and Western standards. Hence, while this was a natural disaster it is clearly also a man-made disaster. While none of the bridge structures had collapsed by the time of the inspections, there are several bridges that had unusual and/or severe damage from the M_w 7.8 earthquake.

Three of the bridges with the most interesting and significant observed damage are presented herein. Bridge 1 formed a plastic hinge 25% up the column height, with vertical rebar buckling and transverse rebar yielding clearly visible, while Bridge 2 has significantly damaged girder ends, with no concrete remaining – just the rebar cage. And, yet, traffic is still flowing across both of these bridges. It is expected that multiple span collapses will happen soon at Bridge 2 from a combination of earthquake aftershocks and repeated live loading, and it should be closed to vehicular traffic. Bridge 1 is a major structure on a busy highway, and it should be assessed by the bridge design group in Türkiye. Future aftershocks could cause a few more nonlinear cycles and failure of the column plastic hinge, resulting in complete collapse of the bridge structure. But other than some minor damage to the abutments, the rest of Bridge 1 appears to be in good condition. A seismic retrofit to the plastic hinge region, or entire column, could save this structure. Because the vertical steel has buckled, in addition to increasing the lateral confinement to the plastic hinge, new vertical steel would have to be added. Bridge 3 had damage to the girder ends as well as to interior and exterior shear keys at the abutments and bents.

Detailed structural analyses have not so far been conducted for the bridge structures of interest because (1) of time constraints for this reconnaissance report and (2) the bridge plans have not yet been obtained from Türkiye. Therefore, the presentation in this report is of observed structural bridge damage and possible explanations for how the damage developed, as well as the level of shaking each bridge experienced based on nearby strong motion station measurements. It is hoped that in the near future the plans for these bridges will be obtained which, in conjunction with the measured ground motions near the three bridges, will allow nonlinear time-history analyses to be conducted, as well as the simpler pushover and spectral analyses, in order to better understand the significant and, in several cases, unusual damage observed.

GPS north and east coordinates, as well as elevations, were determined at the three bridge sites from a Garmin 64S hand-held GPS device (Figure 5-1), allowing the closest free-field strong ground motion station to be found for each bridge, as well as the distances from the bridges to each earthquake epicenter. Bridge 1 was only 18.1 miles (29.2 km) from the epicenter of the M_w 7.8 earthquake, while Bridge 2 was 80.8 miles (130 km) away and Bridge 3 was 81.4 miles (131 km) away. For the M_w 7.5 earthquake, the distances from the epicenter to the three bridges were 64.9 miles (104 km) for Bridge 1 and 134 miles (216 km) for both Bridges 2 and 3. Since all three bridges were significantly closer to the epicenter of the M_w 7.8 earthquake than for the M_w 7.5 earthquake, and because it was the initial and larger event, only the M_w 7.8 earthquake is considered in detail in this report.

Figure 5-1 Garmin GPS Unit used in the field to determine coordinate location of bridges inspected for damage

## 5.2 Measured Free-field Ground Motions near Bridge Structures

Station 2712 was the closest strong motion station to Bridge 1 - 2.00 miles (3.21 km) away. Free-field ground accelerations from Station 2712 during the M_w 7.8 earthquake in the horizontal East-West (EW) and North-South (NS) directions are given in Figure 5-2(a) and (b), respectively. Peak horizontal ground accelerations (PGA) are 0.607 g for the EW direction and 0.565 g in the NS direction, with PGA of 0.354 g in the vertical direction, as seen in Figure 5-2(c). The 5%-damped spectral acceleration graphs for the EW and NS directions are given in Figure 5-3(a), with maximum values of 1.83 g and 1.90 g, respectively. Also shown in Figure 5-3(a) is the smoothed Caltrans, 5%-damped bridge design spectral curve for a M_w 8 earthquake (plus or minus M_w 0.25) having PGA of 0.7 g and a rock or stiff soil profile (Caltrans, 2006) with maximum value of 1.82 g. This Caltrans design curve was obtained from an earlier version of the Caltrans Seismic Design Specifications (SDC) (Caltrans, 2006) since the latest version of the SDC (Caltrans,2019) does not have such a graph readily available for stiff soil and rock sites. Vertical spectral accelerations are given in Figure 5-3(b), with maximum value of 1.37 g.

Station 3124 was the closest strong motion station to both Bridges 2 and 3 at 2.14 miles (3.44 km) from Bridge 2 and 2.33 miles (3.75 km) from Bridge 3. Recorded accelerations versus time at this station from the M_w 7.8 earthquake are given in Figure 5-4(a) and (b) for the horizontal EW and NS directions, respectively. PGAs are 0.659 g in the EW direction and 0.581 g in the NS direction, as seen in Figure 5-4(a) and (b). In the vertical direction the PGA was 0.589 g [Figure 5-4(c)]. Acceleration spectra results with 5% damping are given in Figure 5-5(a) for the two horizontal directions as well as the Caltrans bridge design curve for M_w 8. The vertical direction spectrum is given in Figure 5-5(b). By comparing the horizontal acceleration spectra developed from ground motions measured at Station 3124 to the smoothed Caltrans bridge design acceleration spectrum for M_w 8 and PGA of 0.7 g at a rock or stiff soil site, it is clear that Station 3124 must have a deep layer of soft soil beneath it (or soft soil from the earthquake epicenter to the station) for the peak spectral responses to shift to such long natural structural periods [Figure 5-5(a)]. This is seen in both EW and NS directions.

Therefore, Bridges 2 and 3 are probably on deep, soft soil. In the EW direction the maximum spectral acceleration of 2.15 g [Figure 5-5(a)] was greater than the maximum value of 1.82 g from the smoothed Caltrans design curve for M_w 8 earthquake [Figure 5-5(a)],demonstrating the intense level of shaking that occurred at Bridges 2 and 3. For the NS direction, the maximum spectral value was 1.44 g [Figure 5-5(a)]. In the vertical direction, the peak spectral acceleration was 1.64 g [Figure 5-5(b)], which is important as it implies that the precast girders of both Bridges 2 and 3 lifted off of their simple supports and slammed back down, multiple times, significantly contributing to the observed damage discussed below for both of these bridges, especially for Bridge 2.
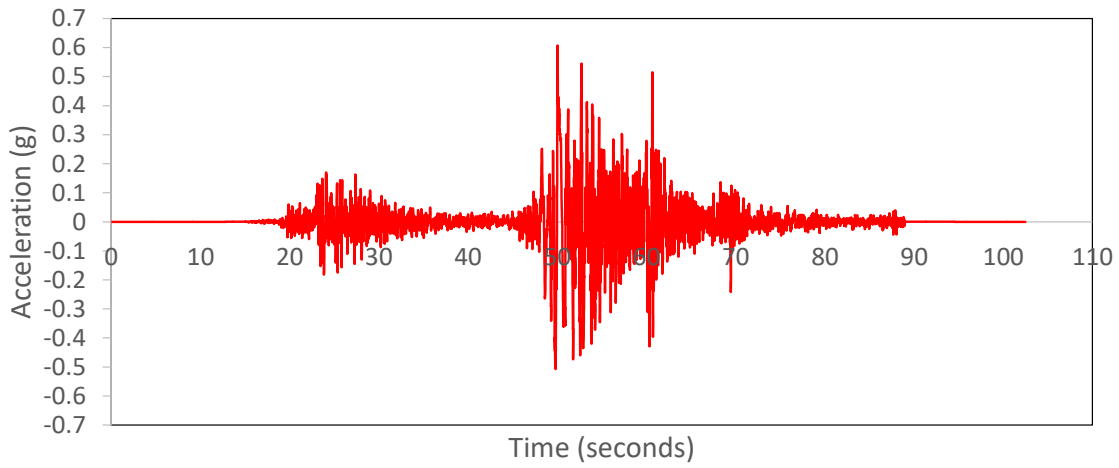
(a) EW direction accelerations versus time
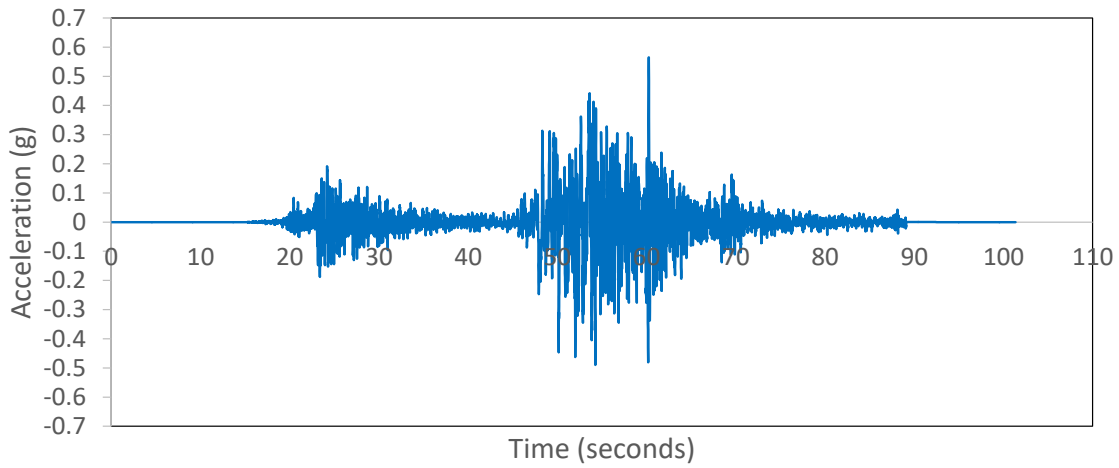
(b) NS direction accelerations versus time
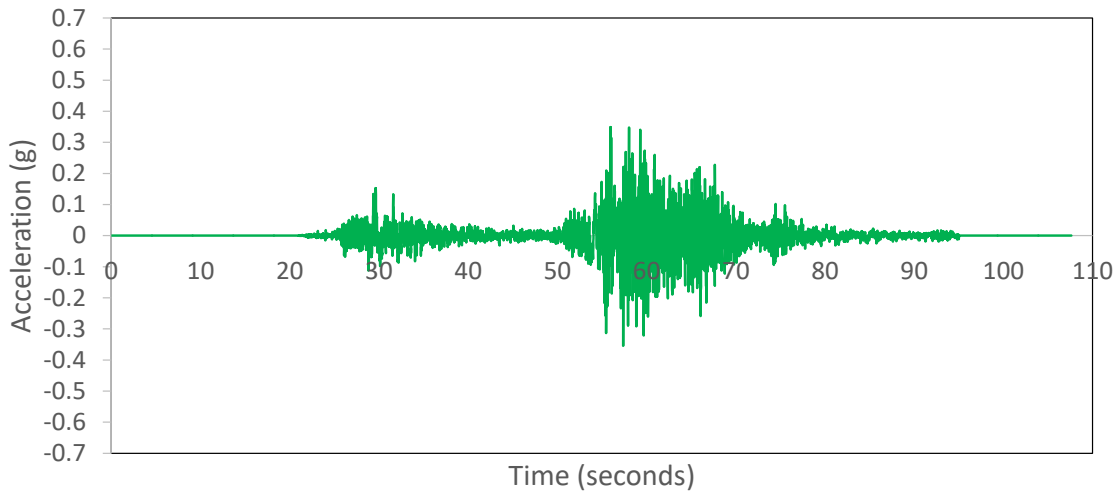
(c) Vertical direction accelerations versus time

Figure 5-2 Station 2712 for Bridge 1, M_w 7.8 earthquake, measured accelerations in all three directions

(a) EW and NS directions, as well as Caltrans Bridge Design Curve for M_w 8 earthquake with PGA of 0.7 g at a rock or stiff soil site

(b) Vertical direction

Figure 5-3 Station 2712 for Bridge 1, M_w 7.8 earthquake 5% damped spectral accelerations

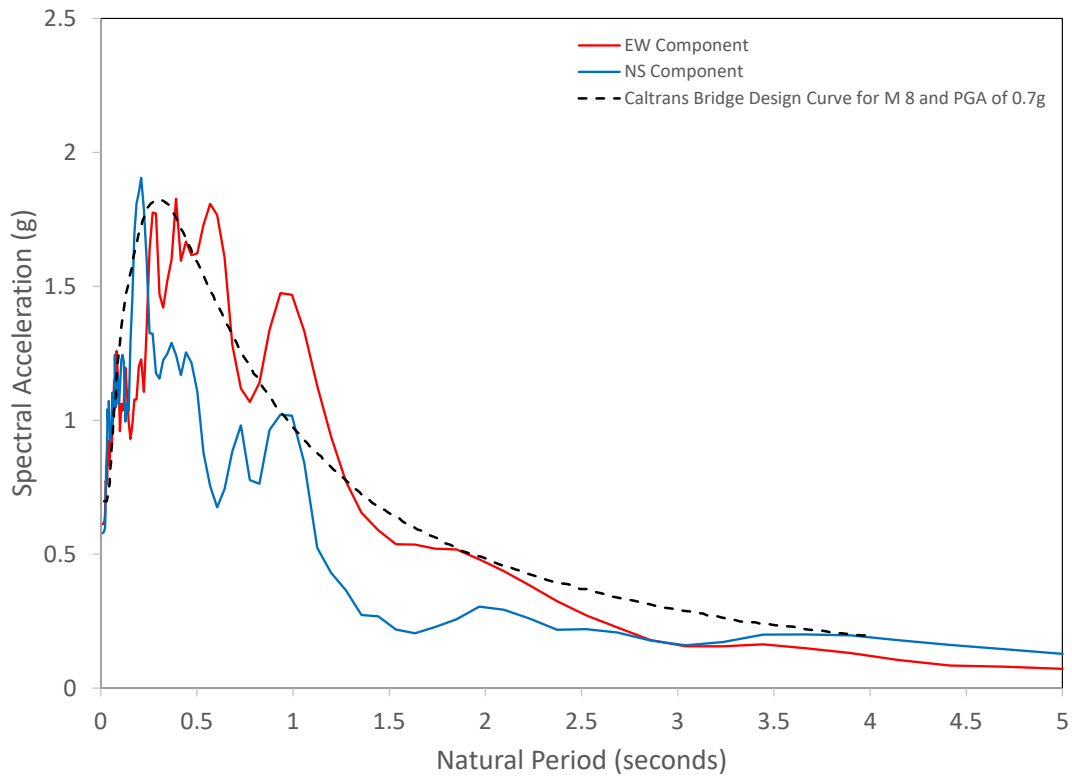(a) EW direction accelerations versus time
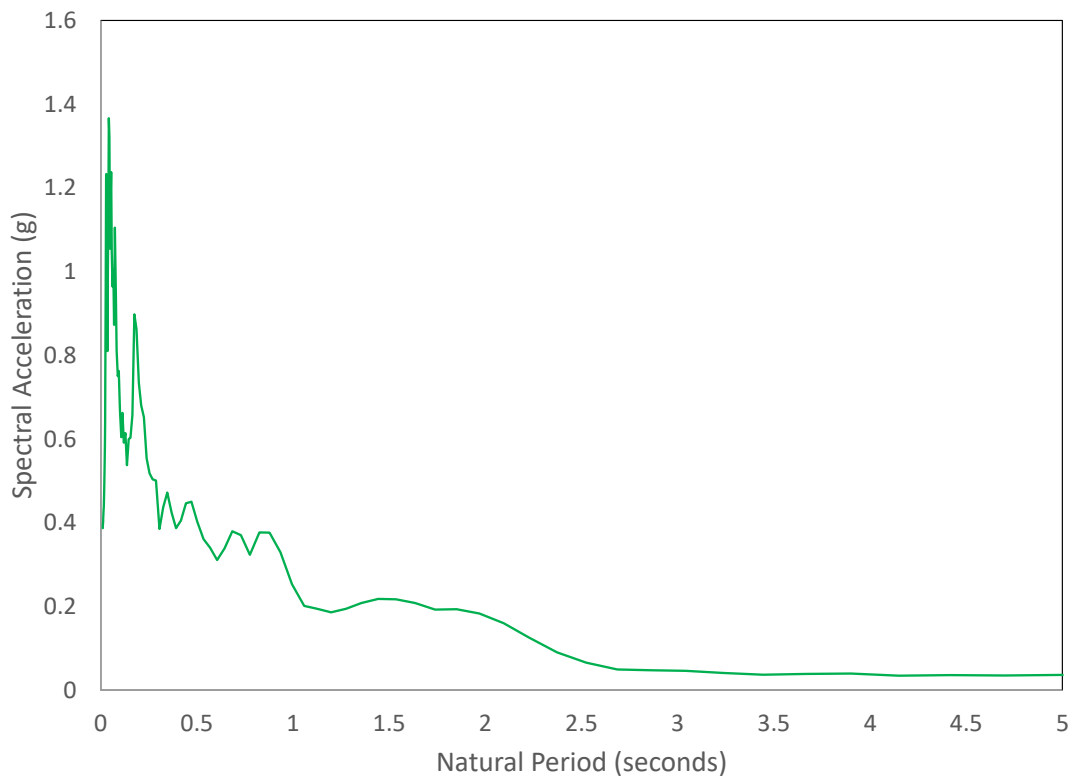

(b) NS direction accelerations versus time

(c) Vertical direction accelerations versus time
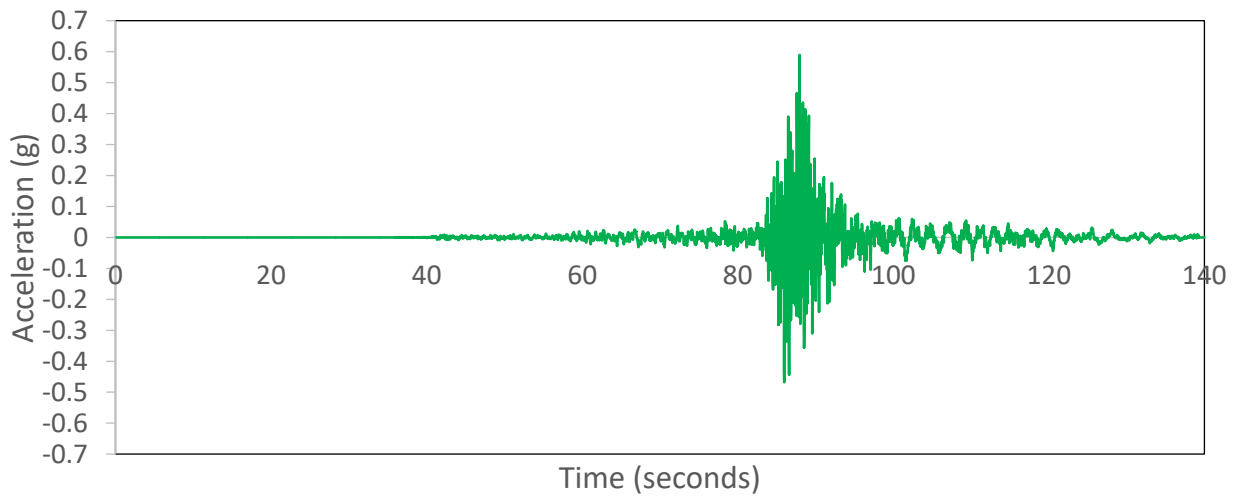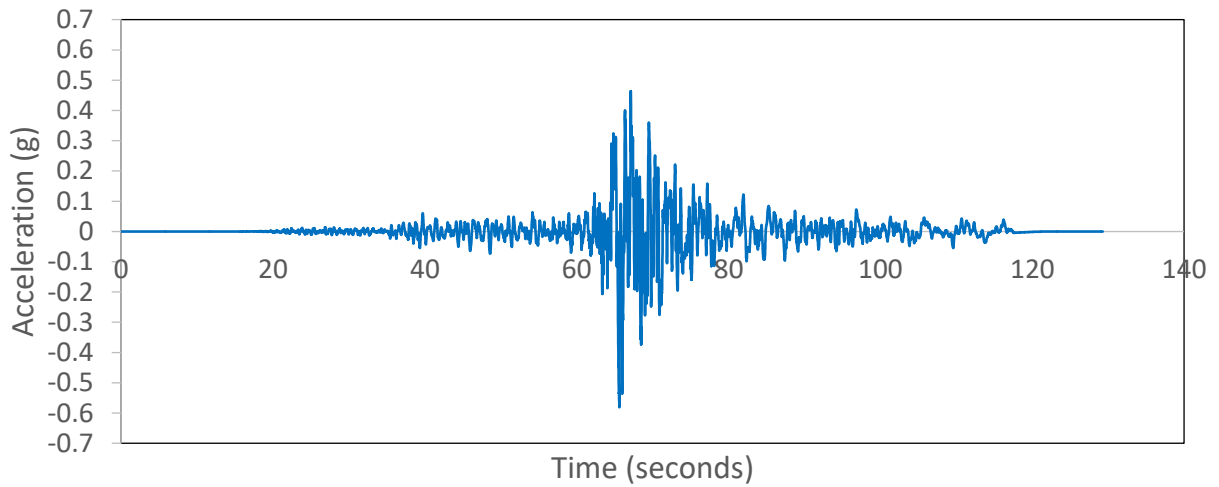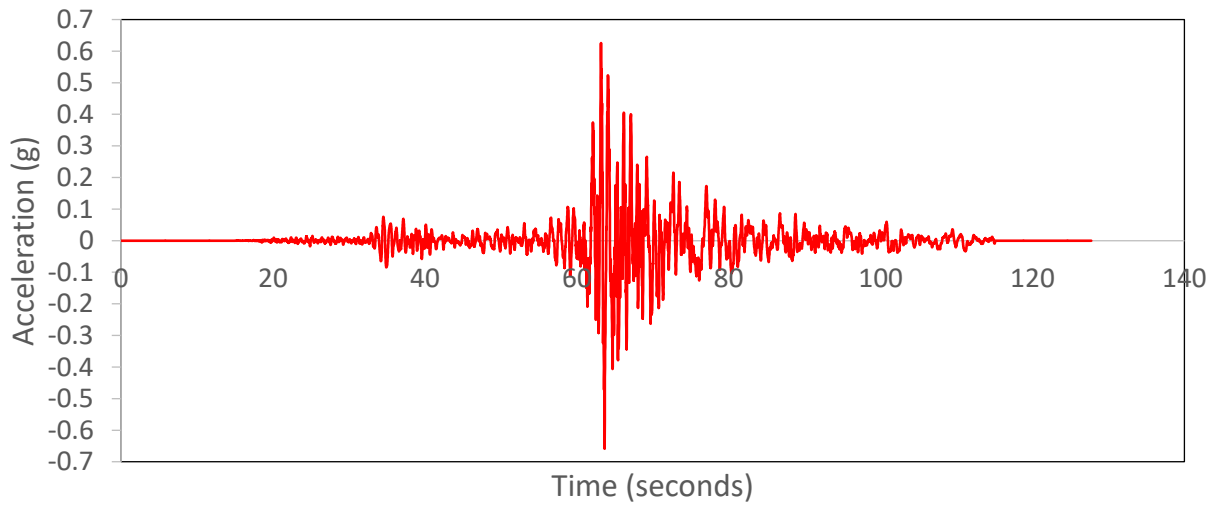
Figure 5-4 Station 3124 for Bridges 2 and 3, M_w 7.8 earthquake, measured accelerations in all three directions
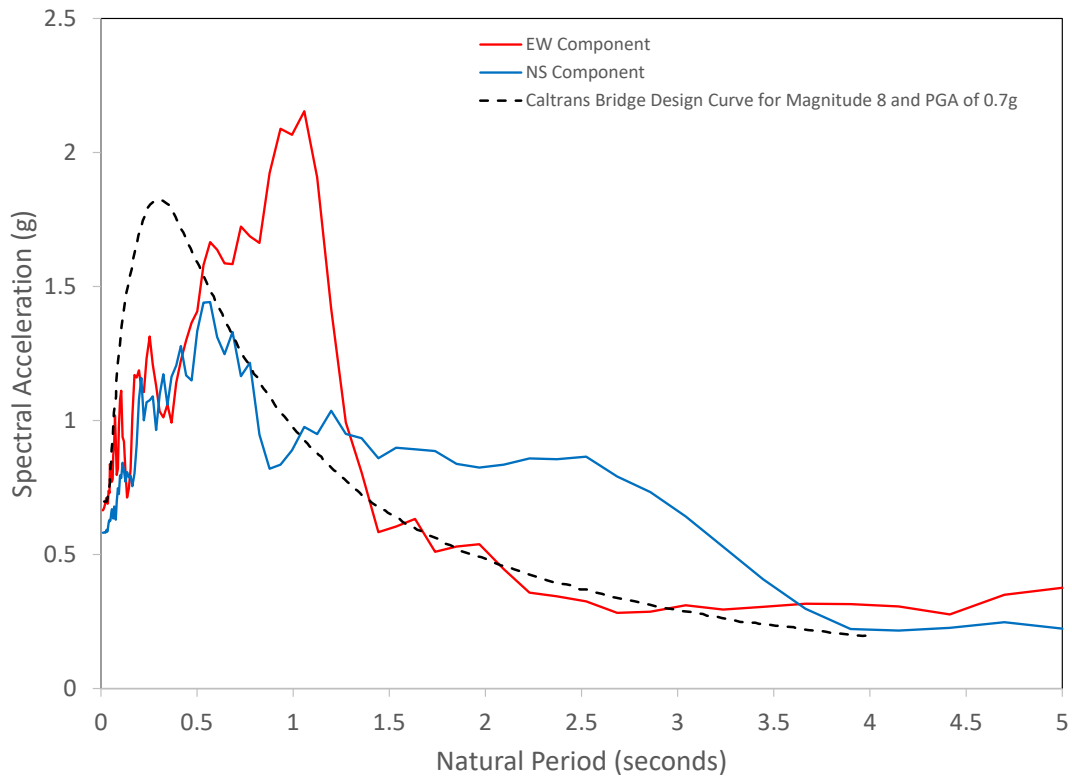
(a) EW and NS directions, as well as Caltrans Bridge Design Curve for M_w 8 earthquake with PGA of 0.7 g at a rock or stiff soil site
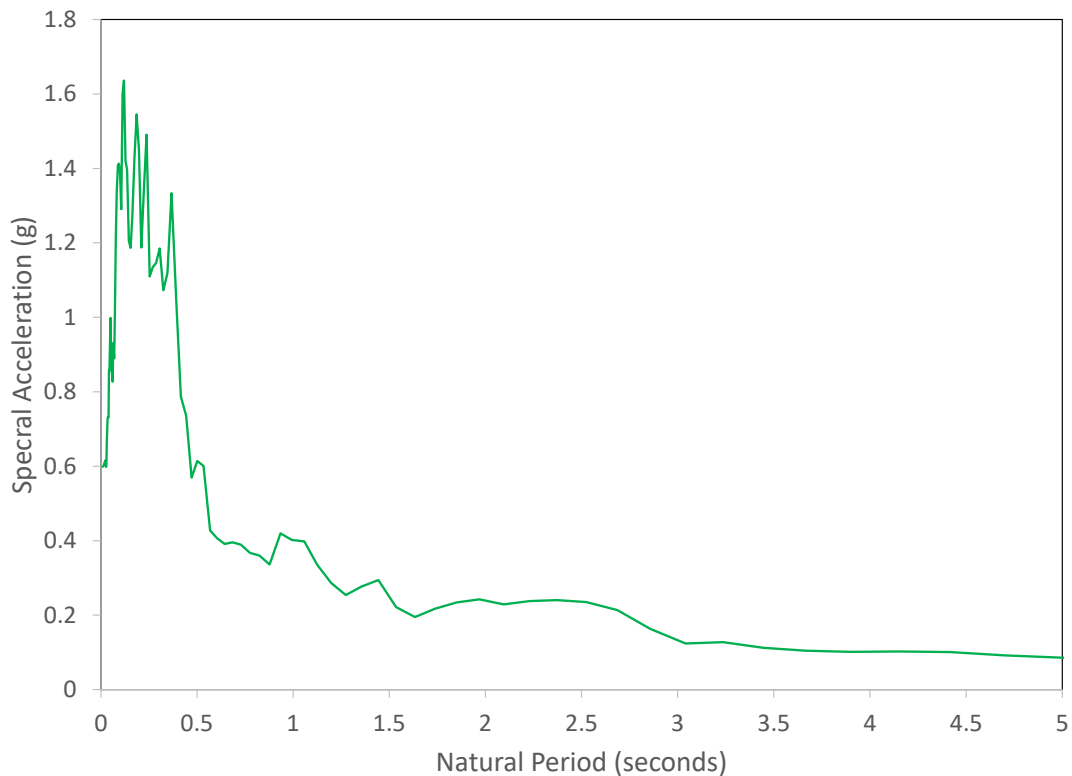
(b) Vertical directions

Figure 5-5 Station 3124 for Bridges 2 and 3, M_w 7.8 earthquake 5% damped spectral accelerations

5.3   Bridge Damage

In the following three sections, three of the bridge structures that were inspected with significant and interesting damage are discussed. While the three bridges were various distances from the epicenter of the M_w 7.8 earthquake, as given above, all three were only a few miles from the fault rupture line.

5.3.1 Bridge 1: Five Span, Prestressed Girder/Steel Girder Superstructure with 10' Diameter RC Columns

The overall impression of the side-by-side structures of Bridge 1 (the Nurdag Viaduct), when looking at them from the above and adjacent roadway, is that they are large structures, with big and imposing circular columns of 10 foot (3.05 m) diameter and height of about 80 feet (24.4 m), with large, square, reinforced concrete (RC) footings, set in an impressive location in the low mountains, with beautiful views of pine trees close to the structures and off to the valley floor in the distance (Figure 5-6). The two parallel and curved five-span bridge structures have single-column-bents with RC columns, RC footings and a combination of precast, prestressed, concrete girders [Figure 5-7(a)] and steel box girders [Figure 5-6, Figure 5-7(b)], at GPS coordinates N 37.17096^0 E 36.69994^0 and elevation of 2563 feet (841 m). It appears that the bearings at the top of the columns may be some sort of isolation system (Figure 5-6), but the bridge plans are needed before this can be verified.

Bridge 1 must have been attacked by severe ground shaking with peak spectral values in both horizontal directions exceeding the maximum Caltrans design value for a M_w 8 earthquake. And while the bridge was damaged, it remains standing, which is the design philosophy for such a large earthquake. The Caltrans bridge design curve for M_w 8 has a scatter of plus and minus M_w 0.25, indicating it is valid for M_w 7.75 to M_w 8.25, with the M_w 7.8 Türkiye earthquake being within this range. Thus, the M_w 8 Caltrans seismic bridge design spectral curve is the appropriate comparison for this earthquake. It is clear that this M_w 7.8 earthquake, that so devastated southern Türkiye, is approximately equivalent to the future "Big One" in California, which has been discussed for many years in California, and elsewhere, by the media, civil engineering profession and people in general. Perhaps California and the rest of the world can now learn some lessons from what happened in Türkiye. The rupture length of 180 miles (290 km) from the M_w 7.8 event is equivalent to the distance from San Diego to Santa Barbara in California, with the City of Los Angeles (LA) right between these two cities.

Figure 5-6 Overall view of bent with 10' diameter RC bridge columns and plastic hinge for one column at about ¼ the way up its height, Bridge 1

(a)   Looking toward abutments of adjacent bridges

(b)   Looking toward opposite abutments of adjacent bridges

Figure 5-7 Overall view of parallel and curved structures of Bridge 1

A single column plastic hinge formed at these two adjacent bridge structures of Bridge 1, but not at the bottom of the column where it is expected and detailed for, since this is where the moment is largest for a cantilever column. The plastic hinge developed in the transverse bridge direction at about ¼ up the height of the column length (Figure 5-6). A side view of the plastic hinge region is given in Figure 5-8. On one side of the plastic hinge the vertical column steel buckled and the transverse steel yielded over several rebar (Figure 5-9), while on the opposite side a large portion of cover concrete spalled off, but with no signs of transverse steel yielding or vertical rebar buckling (Figure 5-10). The most reasonable

explanation for why a plastic hinge occurred 25% up the column height, instead of at the column/footing interface, as expected, is that there were vertical bar cutoffs at this location, reducing the moment capacity to the point that the moment demand/capacity ratio was larger there than at the column base (Figure 5-11).

Spalling of unconfined cover concrete on both sides of this plastic hinge clearly indicates nonlinear cyclic behavior in the transverse direction of the bent, with compressive concrete strains of at least 0.005 (and probably beyond 0.01 based on the observed damage) in both loading directions [Caltrans, 2019, Priestley et al.,1996]. Vertical rebar buckling also shows that nonlinear cyclic behavior occurred, as the steel must yield and reach large strains in tension before direction reversal, which results in compressive stresses and forces in the rebar before the concrete takes any significant compression from the combined section moment and axial force. This phenomenon does not occur under monotonic loading where the concrete is always in compression on one side of the neutral axis [Priestley et al.,1996].

Vertical rebar buckling in a column plastic hinge indicates that it very nearly failed, with only a couple of more cycles needed, which could have resulted in complete collapse of the structure. Note that the spacing of the transverse steel looks good (Figure 5-10), but the bar size appears to be too small for a ductile plastic hinge to develop. This is probably because the plastic hinge was not expected at this location with, perhaps, larger transverse rebar provided towards the bottom of the column. While bar cutoffs is the most likely reason a plastic hinge formed part way up the column height, it is possible that this location had a larger moment demand than at the base of the column due to the combined effects of the transverse mass and rotational mass inertia from the large bridge structure, which is especially important for single-column-bent bridges [Dowell, 2004] since the bridge is free to rotate at the top of the column in the transverse direction as it displaces transversely. Once the bridge plans are obtained, both possibilities can be investigated.

Depending on the size and spacing of the transverse spiral or hoops, vertical rebar can buckle between transverse bars or over many of them, which requires the transverse steel to yield and go into large tensile hoop strains, as is the case for the plastic hinge in Bridge 1. While the transverse rebar is closely spaced (Figure 5-10), the size of the transverse rebar is too small to prevent buckling of the vertical rebar, with the buckled wave occurring over several transverse rebars (Figure 5-8 and Figure 5-9). From the bridge author's experience, good plastic hinge performance for RC bridge columns (cyclic displacement ductility capacity of greater than six) is typically found when the volumetric ratio (percentage) of transverse rebar to the column is about one-half of the volumetric ratio (percentage) of vertical steel to the column. The required minimum amount of vertical steel for a bridge column in California is 1% (Caltrans, 2019), and so the amount of transverse steel should be at least 0.5% for good, ductile column performance. A column with more vertical steel requires more transverse rebar; for example, a column with 2% vertical steel should have about 1% transverse steel. From the images presented here, it appears that the amount of transverse steel was much less than required where the plastic hinge occurred.

Vertical rebar buckling is critical because the rebar strains (tension and compression) on both sides of a buckled wave are very large, resulting in only a few tension/compression strain cycles to cause low-cycle fatigue failure and rupture of the vertical steel. From Figure 5-9, it is clear that the transverse rebar is deformed and at high strains (visibly straight on the sides of the column and tightly curved and bent around the buckled vertical steel), and once the transverse rebar ruptures the core concrete suddenly becomes unconfined, and may not be able to support even the dead load of the bridge structure, resulting in complete bridge collapse. So the combined effects of vertical rebar buckling and fracture after a few cycles, as well as yielding and rupture of transverse rebar, would not only cause the core concrete to suddenly become unconfined, it would provide the wide-open spaces required to allow this now-unconfined and crushed concrete to just pour out of the plastic hinge region. Therefore, future moderate to big earthquakes, or aftershocks, could collapse this large and

important bridge structure by providing a few more cycles to the existing plastic hinge. It is of interest that in the plastic hinge region on the side of the column where the vertical bars did not buckle, the transverse rebar is seen to have constant curvature around the section with nice, even spacing (Figure 5-10 and the left side of Figure 5-8), and no indication of being bent out of position, as is clear on the side of the column with vertical rebar buckling (Figure 5-9 and the right side of Figure 5-8). In addition to the column plastic hinge discussed above, damage and spalling at the abutment from longitudinal and transverse banging of the superstructure was evident (Figure 5-12).

Figure 5-8 Side view of plastic hinge region of 10' diameter RC bridge column, Bridge 1

Figure 5-9 Close-up view of column plastic hinge, with buckled vertical rebar and yielded transverse rebar, Bridge 1

Figure 5-10 Close-up view of column plastic hinge, spalling of cover concrete (opposite side to where vertical bars had buckled), Bridge 1
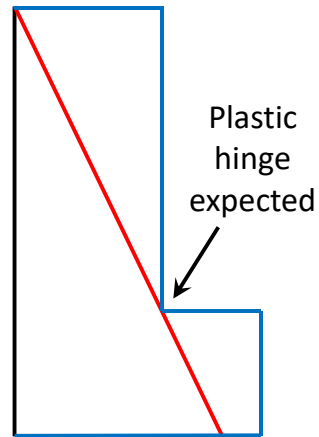
Figure 5-11 Column moment demand and moment capacity when bars are cutoff at ¼ location of the column height, Bridge 1

Figure 5-12 Damage at abutment, Bridge 1

5.3.2 Bridge 2: Six span, Precast, Prestressed I-Girder Superstructure with RC Columns

These two parallel and straight bridges (Asi Bridge) are over water (Asi River) and located at GPS coordinates N 36.25505^0 E 36.20430^0 and elevation of 315 feet (96 m). They consist of precast, prestressed, I-girders with RC topping slab, AC overlay and RC columns (Figure 5-13).

Figure 5-13 Overall view from under Bridge 2

Lateral motion of the bridge caused severe damage and failure of external shear keys (Figure 5-14 through Figure 5-16). Combined lateral, longitudinal and vertical motion resulted in many rubber bearing pads that had supported the simply supported girders to fall to the ground (Figure 5-17 shows one). End regions of many of the precast concrete girders

were significantly damaged from large vertical (as well as longitudinal and horizontal) accelerations and forces, including impact, resulting in shear cracks and extensive spalling of the concrete, as shown in Figure 5-18 through Figure 5-20. The spalling reached a long distance out into the girders (Figure 5-18 and Figure 5-20), far beyond the supports. In many cases there was no concrete left, with just the rebar cage remaining toward the girder end (Figure 5-19) supporting the end shears. This brings up an interesting question as to what happened to the prestressing strands, and associated prestressing force, as the concrete around the strands spalled out. A coiled-up prestressing strand was found adjacent to one of the bridge abutments that had flown out of a girder (Figure 5-21 and Figure 5-22).

The extensive damage to the ends of both internal and external girders appears to be a result of a sequence of events; first diagonal shear cracks form just beyond the supports from large vertical accelerations and forces, including multiple impacts from girder-end liftoff and slamming back down (peak vertical spectral acceleration is 1.64 g at this bridge), then concrete begins to spall off at the girder ends due to the combined effects of the large vertical, transverse and longitudinal forces, including impact in all three directions. With no concrete left at the girder ends there is nothing to hold the prestressing steel to the girder end region, with the transfer length moving forward to where there is still concrete, causing added damage to the already cracked and spalled girder end region, with more spalling and slip, and so on, until a much longer distance of damage has developed than from just diagonal shear cracking. As seen in Figure 5-18 and Figure 5-20, the spalled region at the girder ends is very long for exterior girders, with similar damage occurring to interior girders (Figure 5-23 through Figure 5-25). Vertical rebar buckling in the web of the girders [Figure 5-24] contributed to the extent of the spalling. Severe twisting and bending of one precast girder happened, as seen in Figure 5-26 through Figure 5-28.

Plastic hinges developed at the base of the columns in the longitudinal direction, which is the weak column direction (Figure 5-29). Settlement occurred at both approaches to the bridge (Figure 5-30 and Figure 5-31), requiring vehicles to slow down to enter and exit the structure. However, traffic should not be allowed on this bridge as it is just a matter of time before complete span collapses occur from continued traffic loading and/or earthquake aftershocks due to the poor condition at many of the girder ends.

Figure 5-14 Failed exterior shear keys, Bridge 2

Figure 5-15 Closer view of failed exterior shear key and end-of-girder damage, Bridge 2

Figure 5-16 Another view of failed exterior shear keys, Bridge 2

Figure 5-17 Rubber bearing pad on ground; one of many, Bridge 2

Figure 5-18 Damage to end of precast girder, Bridge 2

Figure 5-19 Closer view of damage to end of precast girder, Bridge 2

Figure 5-20 Damage over long range to end of exterior precast girder, Bridge 2

Figure 5-21 Prestressing cable at end of precast girder, Bridge 2

Figure 5-22 Close-up view of prestessing cable near end of precast girder, Bridge 2

Figure 5-23 Interior girder damage at end of precast girder, Bridge 2

Figure 5-24 Close-up view of interior girder damage at end of precast girder, Bridge 2

Figure 5-25 Significant interior girder damage at end of precast girder, Bridge 2

Figure 5-26 Significant interior girder damage at end of precast girder, Bridge 2

Figure 5-27 Closer view of significant interior girder damage at end of precast girder, Bridge 2

Figure 5-28 Lateral/vertical bending and damage of interior girder at mid-span and shear key damage at girder end, Bridge 2

Figure 5-29 Plastic hinging at base of RC column, Bridge 2

Figure 5-30 Settlement of approach to bridge, View 1, Bridge 2

Figure 5-31 Settlement of approach to bridge, View 2, Bridge 2

5.3.3 Bridge 3: Six span, Precast, Prestressed I-Girder Superstructure with RC Columns

These two parallel and curved bridges have six-spans with 11 precast, prestressed, I-girders per span and RC columns (Figure 5-32 and Figure 5-33), located at GPS coordinates N 36.24060^0 E 36.21406^0 and elevation of 336 feet (102 m). Damage observed for Bridge 3 includes cracking and spalling at the ends of the precast girders (Figure 5-34 and Figure 5-35), as well as failure of external (Figure 5-36) and internal shear keys (Figure 5-37). The maximum vertical ground acceleration recorded for this bridge was 0.589 g, with peak vertical spectral acceleration of 1.64 g. This indicates that the shear forces at the ends of the simply-supported precast girders were much larger than from just the static dead load of the structure, and that the girders were lifting off of the supports and slamming back down, resulting in impact shear forces that were larger than the girders were designed for, causing the shear cracking and concrete spalling seen at the girder ends (Figure 5-34 and Figure 5-35), which is similar to, but not as severe as, what was observed at Bridge 2.

Figure 5-32 Overall view of Bridge 3

Figure 5-33 View under Bridge 3, showing 11 precast I-girders per span for each bridge

At the same time that the girders were being lifted off of their seats and slammed back down again, large horizontal and longitudinal forces were occurring, adding to the damage at the girder ends, and causing the shear key damage and failures that were observed (Figure 5-36 and Figure 5-37). Since the precast girders are only connected to each other through the cast-in-place (CIP) topping slab, they are free to move about almost independently of each other away from the deck. Adding at least one diaphragm along the length of each span would have helped the bridge move as a unit rather than as independent precast girders, which would have been even more important for Bridge 2.

Figure 5-34 Damage at end of Bridge 3 precast girders

Figure 5-35 Close-up view of damage at end of Bridge 3 precast girder

Figure 5-36 Damage of external shear key at Bridge 3 abutment

Figure 5-37 Damage of internal shear key at bent of Bridge 3

6 PERFORMANCE OF INDUSTRIAL BUILDINGS

6.1 Precast Concrete Buildings

In Türkiye, industrial buildings are predominantly constructed using RC precast structures. This type of building system provides various benefits, such as speedy construction, lower project costs due to prefabrication, adherence to high quality standards, and improved safety. These benefits make this type of construction attractive and popular for industrial purposes. However, the static scheme commonly used in this type of construction also has a major drawback that affects its seismic performance. For single-story industrial buildings in Türkiye, precast reinforced concrete long-span roof girders are supported by cantilever precast columns, which allow for large, open spaces necessary for manufacturing activities (Saatcioglu et al., 2001). This is the most frequently used typology for this type of construction, and it was also observed in the Turkoglu Organized Industrial Zone (OIZ), which was affected by the 2020 Elazig earthquake.

The buildings had one-story industrial structures with large spans and heights. The typical span lengths of the main direction were about 15 m to 25 m, while the other direction had span lengths of around 8 m. The story heights varied from 7 m to 10 m [see Figure 6-1(a), Figure 6-2(a) and Figure 6-3(a)]. The structures consisted of precast columns, beams, roof girders, purlins, and wall panels that related to pin connections. Columns were fixed to precast pocket foundations with grout to provide a rigid base for the structure, as shown in [Figure 6-1(a) and (b)]. Some of the column ends formed plastic hinges due to the bending moment induced by the earthquake loading, as shown in Figure 6-1(c). The roof had long-span girders that were placed along the transverse axis of the building and were simply supported by column corbels without any moment connection. The depth of these girders varied along their span, resulting in a triangle configuration (double-slope girders) that had low torsional stiffness and strength. Beams were placed along the longitudinal axis of the building and were seated on the column capitals with vertical steel dowels that provided shear resistance only. Purlins were placed between the roof girders at regular intervals and supported the roof panels. Prefabricated roof girders, gutter beams, and purlins were not connected to each other or to the columns and beams at both ends, as shown in [Figure 6-1(c) and (d)].

(a)

(b)

(c)

(d)

Figure 6-1 Damage of precast building (a) undamaged portion of the precast building, (b) damaged portion of the precast building, (c) corbel damage and plastic hinging of column, (d) precast slab failure

(a)   (b)

Figure 6-2 Damage of Precast buildigs in Turkoglu OIZ (a) precast tapered beam failure owing to the loss of support, (b) cladding pannels due to panel-to-structure failure

(a)   (b)

Figure 6-3 Damage of Precast buildigs in Turkoglu OIZ (a) damaged portion of the precast building, (b) precast tapered beam failure owing to the loss of support

The industrial building (that was under construction) collapsed due to unseating of the girder ends or from the beams rotating over the column capitals. Because the first portion of the structure operated successfully, as shown in Figure 6-1(a), the failure was considered to have started at the pin connections, which were not properly secured since they were still under construction. The roof was constructed out of lightweight materials, such as sandwich panels with polystyrene foam core, which did not provide sufficient diaphragm action to distribute the lateral loads and prevent out-of-plane instability of the girders. Furthermore, as indicated in Figure 6-2(b), precast concrete wall panels were commonly used for the external walls of Turkoglu OIZ. The connection details for the wall panels were normally designed so that the panels did not contribute to the lateral stiffness of the building; however, the existing industrial precast concrete buildings in the affected area did not meet this principle, resulting in detachment of the exterior cladding elements as shown in Figure 6-2(b). Another example of not sufficient diaphragm action can be seen in Figure 6-3(a). As indicated in Figure 6-3(b), the roof was made of light materials, like sandwich panels with foam inside, that did not help to spread the sideways forces and stop the girders from bending out of shape.

6.2 Reinforced Concrete Buildings

Three reinforced concrete industrial buildings were investigated during the six-day structural seismic reconnaissance (see Figure 6-4). The buildings were not accessible for inspection, so the condition of the interior structures could not be assessed. Figure 6-4(a) shows a damaged reinforced concrete building (Coordinates: 37.45764°N, 37.25636°E) that suffered from joint failure. The building was constructed before 2000 and fortunately no fatalities were reported. The reinforcement detailing of the joints is crucial to provide continuity and load transfer across the joint; therefore, a deficiency of reinforcement can cause unexpected stress concentrations that lead to cracking and failure of the joint. The figures indicate that the rebar slipped out of the joint, which might have occurred due to insufficient reinforcement development length, which is required to transfer the loads from the rebar to the concrete effectively. Another factor that might have contributed to this failure is the quality of materials used in the construction of the joint.

Figure 6-4(b) and (c) show similar damaged reinforced concrete buildings that collapsed due to the large mass at the roof. They were also built before 2000 and luckily no fatalities were reported (Coordinates: 37.19352°N - 036.57438°E) for

Figure 6-4(b) and 36.59820°N - 36.19591°E for Figure 6-4(c)]. The damage observed in these buildings was caused by a storage tank or a heavy mass on the roof that fell over during the earthquake. The reason for the fall-over might be the high vertical acceleration observed from the earthquake, which causes extra weight of the storage tank or mass due to the vertical component of the earthquake. This extra weight may not have been considered during the design process of the roof structure. On the other hand, the inertial forces at the top part of buildings due to amplification of the horizontal component of the earthquakes are higher than at the lower stories. High lateral acceleration demand at the top might have caused shear connection failure between the roof structure and the columns.
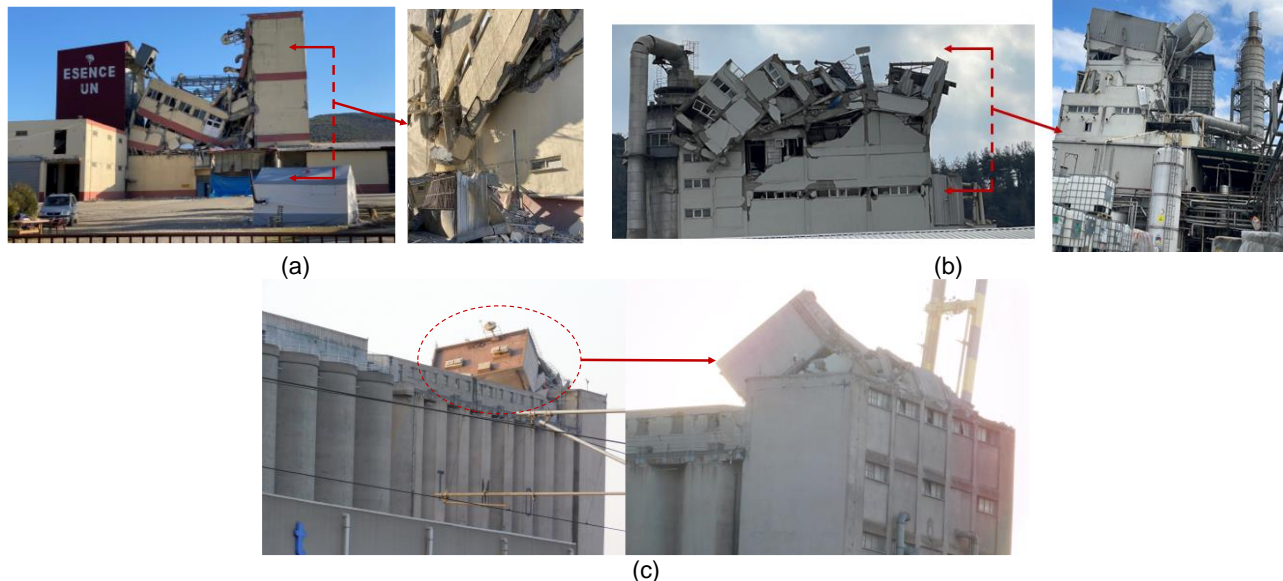

(a)

(b)

(c)

Figure 6-4 Damage of RC buildings (a) to (b) Essence Un, (c) and (d) ABC Deterjan, (e) Toprak Mahsulleri Ofisi (TMO)

6.3   Steel Structures

Hybrid structures are structures that combine steel members with reinforced concrete or precast frames for industrial purposes. Full steel structures are not commonly used in Türkiye due to their high cost and low fire resistance. Instead, a combination of steel members with reinforced concrete or precast frames is generally used for industrial structures, as they provide more flexibility and economy. During the reconnaissance, only two buildings constructed with a combination of concrete and steel were found in the affected areas. The first structure was under construction at the time of the earthquake in Turkoglu OIZ [Coordinates: 37.33625 °N and 36.81581 °E]. As illustrated in [Figure 6-5(a) and (b)], the gravity-load framing system of this construction consists of a steel space frame that is supported by steel trusses that span between reinforced concrete columns. For the extension of corbels, short steel columns were utilized on top of the reinforced columns. This type of structure is rather widespread in Turkoglu OIZ, as it allows for large open spaces and easy installation. Overall, the roof frame behaved well during the earthquake; nevertheless, tilting of the steel truss beams was noted, as shown in Figure 6-5(c). This might have occurred due to insufficient bracing or connection details. The light roof covers that were temporarily attached to the roof collapsed, causing buckling at one of the bracings [see Figure 6-5(d)]. This might have occurred due to poor quality or installation of the roof covers.

Another hybrid structure is owned by Iskur and located in Kahramanmaras [see, Figure 6-6(a), Coordinates: 37.55340°N and 36.96157°E]. One of the factory's buildings was exposed to multi-hazard, as shown in Figure 6-6(b). The factory was not damaged structurally by the earthquake; however, a spark at the generator during the earthquake created a fire, which quickly became uncontrollable due to the extremely combustible materials they were using in their production process. The fire spread rapidly and engulfed the whole building, causing severe damage to the structure and its contents. When the steel temperature rises due to fire exposure, corrosion, dimensional changes, and permanent changes in the steel microstructure occur, resulting in a reduction in steel modulus of elasticity and strength, and ultimate collapse of the structure [see Figure 6-6(c)]. This shows the importance of fire protection and prevention measures for hybrid structures.

(a)

(b)

(c)

(d)

Figure 6-5 Damage of steel roof system including reinforced concrete columns (a) overall view of structure, (b) hybrid structure, (c) steel truss tilting, (d) buckling at the brace dur to collapsing of light roof covers

<div style="text-align:center">(a)</div>

<div style="text-align:center">(b)</div>

<div style="text-align:center">(c)</div>

Figure 6-6 Multi hazard on steel suspended ceiling structural system (a) Prior to earthquake, (b) After the earthquake and fire, (c) Detailing

6.4   Silos

Silos are essential for the food industry and other sectors that rely on bulk materials. Failure of these structures could disrupt the food chain or cause collateral damage including fires, explosions, and the release of hazardous substances into the air or soil. As a result, understanding the behavior of these structures when subjected to seismic loads is crucial for their design and maintenance. An earthquake ground motion contains three components that result in structural loads in three directions: vertical, and two horizontals. Vertical seismic loads have a minor impact on relatively heavy silo structures; however, lateral loads can significantly impact taller silos storing heavier contents. The magnitude of the horizontal seismic load is related to the silo's weight and the seismic intensity. The height of the silo structure's center of mass rises as the height of the silo rises. Considering that the horizontal seismic load is applied nearly at the center of mass, the moment arm for the lateral load and the associated moment at the base increases. The higher moment causes a nonuniform pressure distribution at the base of the silos, which can be substantially more critical than the pressure induced by gravity loads. This can lead to buckling or cracking of the silo walls or foundations. Figure 6-7(a) shows significant buckling at the bottom end of the silos and failure of arches that formed inside the silos due to improper flow parameters. If the flow parameters of the bulk material being handled in a silo differ from, or have greater changes than, those for which the silo was intended, obstructions such as arches and ratholes may form, and the flow pattern and loads may be entirely different than anticipated (Carlson and Holmes, 2003). These obstructions can cause uneven distribution of loads inside the silos and increase the risk of structural failure. Many steel silos in the Nurdagi region were subjected to elevator failure, as shown in Figure 6-7(a), which caused dynamic loading to silos that lead to total or partial collapse of the structure. Smaller, elevated, cylindrical metal silos are often supported on local brackets attached to the side of a shell (Doerich and Rotter, 2008) which causes linear-elastic deformations and bifurcations. Figure 6-7(b) shows the deformation at the supporting system of a small metal silo. One of the metal silos totally collapsed due to the overturning moment of the structure while the other one formed flexural buckling at the supporting system. Brittle welded connection failure was observed at the supporting system of the metal silo. The damage to the concrete silo was concentrated in the walls near the bottom of the silos, as shown in Figure 6-7(c). Severe concrete crushing, lack of sufficient reinforcement, steel bar fractures and buckling were observed.
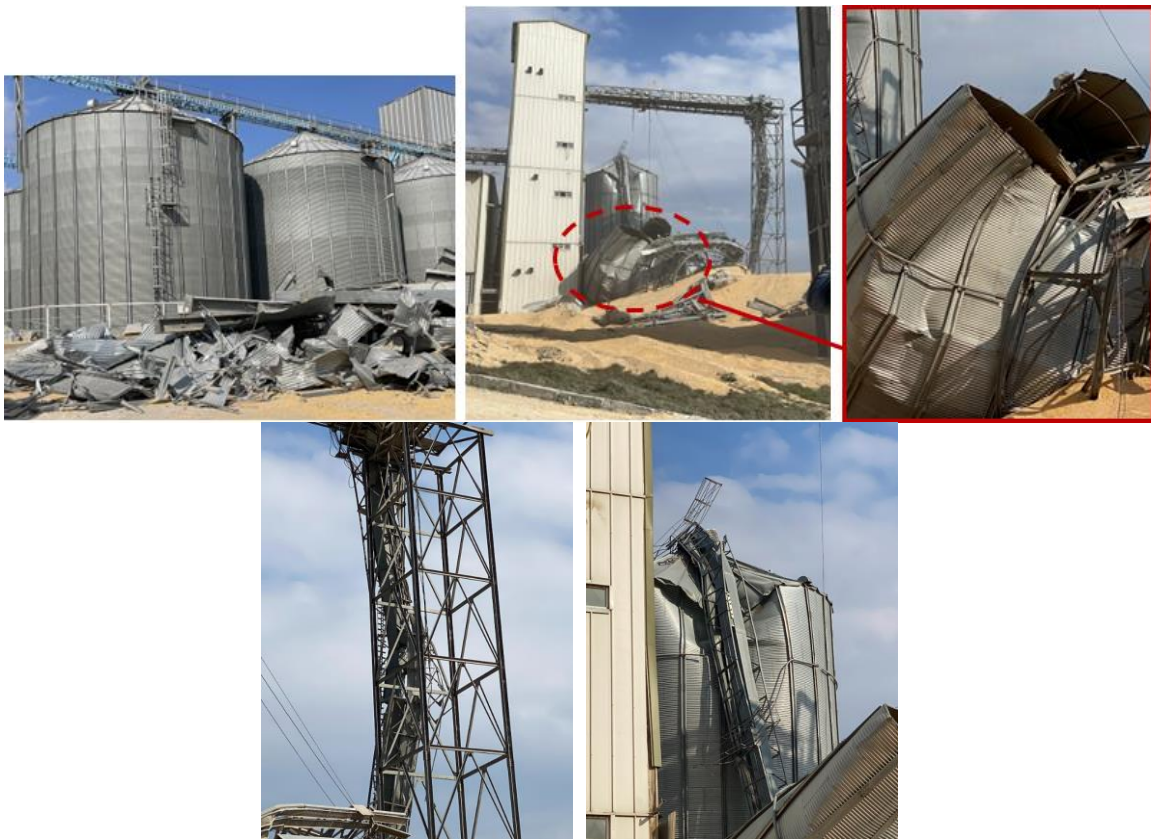
Figure 6-7 Damage of Silos (a) Corn silos, (b) Total collapse of a slender metal silo due to brittle welded connection, (c) concrete spalling on silos

7   CRITICAL FACILITIES

7.1   Schools

In Türkiye, a national policy is in place to mitigate earthquake impacts and enhance preparedness at national, regional, local, workplace and family levels. This policy includes pre-earthquake inspection of critical infrastructure (i.e., schools and public buildings) and prioritization for strengthening based on relative risk scoring. This policy was adopted after the 1999 Izmit earthquake, which killed over 17,000 people and exposed the vulnerability of many buildings that did not comply with seismic codes. School buildings in Golbasi and Iskenderun, where liquefaction is the main problem in the region, were investigated during the reconnaissance. Liquefaction is a phenomenon that occurs when loose and saturated soil loses its strength and stiffness under seismic shaking and behaves like a fluid. This can cause severe damage to buildings and infrastructure. Settlements in a garden wall [see Figure 7-1(a), Coordinates: 36.59325°N and 36.16602°E] damage to non-structural elements, such as infill walls [see Figure 7-1(b), Coordinates: 36.55244°N and 36.15448°E], as well as heavy equipment movement that was observed on several occasions, pose a threat, particularly in schools, for the lives of students. Fortunately, schools were just recently closed at the time of the earthquake; however, the observations above highlight the necessity of pre-earthquake assessment of potential nonstructural damage and the need for mitigation measures. According to the president of Dr. Gani Bahadirli Elementary School, most schools in the Iskenderun area had been seismically retrofitted in the previous seven years. As a result, most schools in the region suffered limited, to no, damage. Those that have not yet been retrofitted suffered severe damage, such as the collapse of the conference room in the additional building of Mithatpasa Primary School, as depicted in Figure 7-1(c) (Coordinates: 36.59121°N and 36.16785°E).

(a)

(b)

(c)

Figure 7-1 Performance of schools in Iskenderun (a) Pre-school, (b) Retrofitted elementary school, (c) Unretrofitted elementary school

7.2   Place of Worship (Mosques and Churches)

Worship structures are significant because they have the capacity to accommodate large groups of people who need to stay safe and warm after an earthquake. As a result, their performance is critical not only during an earthquake, but also after earthquakes to ensure that operations continue uninterrupted. In numerous occasions, in the Kahramanmaras and Osmaniye regions, the most vulnerable part of a mosque's minaret toppled over while the rest of the mosque was not affected. The minaret is a tower attached to the mosque from which the call to prayer is announced. It is one of the most visible aspects of mosque architecture and varies in shape and style depending on the region and period. The minaret is attached to the mosque at the second story level, which causes stiffness and boundary variation in the height, resulting in cracks, typically at areas with abrupt cross-sectional changes, which causes the minarets to fall. Figure 7-2(a) illustrates the partial collapse of the minaret from where this cross-sectional change begins. Serious damage and failure of the mosque was found in Golbasi and Iskenderun, where settling was the primary cause. When soil supporting foundations is subjected to excitation during an earthquake, it may experience consolidation or shear failure, resulting in ground settlement or subsidence. Ground settlement can cause buildings to shift, resulting in masonry wall damage, as demonstrated in Figure 7-2(b) and Figure 7-3 for a mosque and church, respectively. According to locals, the dome of St. Ilyas church (Coordinates: 36.09764°N and 35.99159°E) suffered moderate damage after the main shock and collapsed following the Samandagi earthquake [February 20th, 2023, see Figure 7-3(a)]. The church was originally built as a Byzantine church in the 6th century CE and later converted into a mosque by the Ottomans in the 16th century. It is one of the oldest surviving monuments in Türkiye and an example of how religious buildings reflect the cultural changes that have occurred in the region over time.

(a)

(b)

Figure 7-2 Damage of Mosques (a) Haci Murat Mosque in Kahramanmaras, (b) Merkez Cumhuriyet Mosque in Pazarcik

Figure 7-3 Damage of Churches (a) St. Ilyas Church in Samandagi, Antakya, (b) Roman Catholic Church in Iskenderun

7.3 Hospitals

Emergency management is crucial in limiting a disaster's impact and saving lives. Hospital infrastructure, road viability, search and rescue teams, civil protection activities, helicopter medical evacuations and, most importantly, field hospital facilities all play a role in emergency management. Several components of response management are interconnected. As a result, during a crisis, all components must work efficiently and effectively while considering the consequences of the others. As the primary component of emergency management, hospitals should be designed to handle large numbers of victims during and after natural disasters. However, many hospitals in Türkiye are vulnerable to earthquake damage due to their age and lack of seismic retrofitting. Hospitals in Kahramanmaras and Iskenderun were checked, and it was discovered that a couple of old state hospitals were moderately damaged during the two large earthquakes on February 6th, forcing the hospitals to evacuate following the incident [see Figure 7-4(a)]. This disrupted the health care services and increased the risk of infection and mortality among the patients. To prevent such situations, Türkiye has adopted a national policy to mitigate earthquake impacts and enhance preparedness at national, regional, local, workplace and family levels. This policy includes pre-earthquake inspection of critical infrastructure (i.e., schools and public buildings) and prioritization for strengthening based on relative risk scoring. This policy was implemented by the Disaster and Emergency Management Authority (AFAD), which was established in 2009 as a single government institution to coordinate and exercise legal authority in cases of disaster and emergencies. In the preceding decade, the General Directorate of Health Investments of the Ministry of Health chose to develop new city hospitals with seismic base isolators to limit earthquake damage in high seismic zones. Figure 7-4(b) depicts a friction pendulum bearing seismic isolator used in the Malatya City Hospital addition. During the earthquake, the existing major part of Malatya City hospital performed admirably.
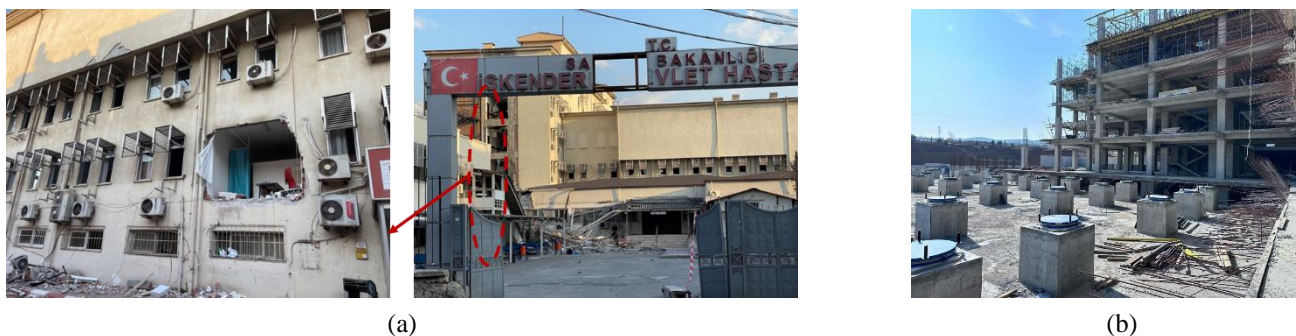

Figure 7-4 Hospitals (a) Old state hospital in Iskenderun, (b) New city hospital in Malatya

8   LESSONS AND CONCLUSIONS

On February 6, 2023, an earthquake sequence struck Kahramanmaras with magnitudes of M_w 7.8 and M_w 7.5, affecting a total of ten different cities with a combined population of 15 million people. The reconnaissance team inspected structural and geotechnical damage for two weeks in the field, starting one week after the main shock. The team visited several towns and cities, including Iskenderun, Antakya, Osmaniye, Kahramanmaras, Gaziantep, Nurdagi, and Golbasi. The structural damage observed in the inspected structures was mainly due to disparities between the seismic code requirements and the design/construction practices of the damaged buildings. In situ mixed concrete with low strength (i.e., 6-10 MPa) was used in the construction of the damaged buildings. Poor workmanship and a lack of oversight during the construction process likely led to construction practice issues that resulted in extensive damage to reinforced concrete (RC) residential buildings. Many older buildings exhibited stirrups bent with 90-degree hooks, unengaged stirrups, large stirrup spacing, and the absence of cross ties. These improper details not only jeopardize the section's integrity but also result in shear failure and limited ductility capacity of RC members, as observed in previous catastrophic events in Türkiye.

Most residential building failures and related deaths occurred in a particular type of construction used throughout Türkiye, consisting of a RC frame of columns and girders, and infill walls of bricks or masonry blocks with no gaps between the walls and the frame. The infill walls are not connected to the frame members, and the bricks or masonry blocks are not tied to each other. As a result, the infill walls are not considered in seismic design as part of the lateral load-resisting system. However, the diagonal shear cracks seen on almost all infill walls for most of these buildings indicate that these walls are resisting lateral loads before they fail and force the RC frame to suddenly take the earthquake loads. The combined response of the frame and infill walls is much stiffer than the frame acting alone, causing amplification of the earthquake loads above what is considered in the design, leading to the failure of these building types. Infill walls can also cause a short column effect, with larger shears than expected from the full column assumption. Additionally, many building failures were due to soft soil and liquefaction of sandy soils, related settlement, and building structures rotating as a unit about their foundations. Sand boils, liquefaction, lateral spreading, settlement, and multiple wide-open, deep cracks in the soil were observed in several locations.

While thousands of residential buildings, mosques, churches, silos, and industrial buildings collapsed, there were no bridge failures as far as the reconnaissance team knows. Several bridge structures had severe damage, as expected under such an extreme event, but they remained standing. Although many RC buildings with infill walls failed, some heavily damaged buildings remained standing, with girder and column plastic hinges forming in critical locations properly. Prior to rebuilding, it is recommended to consider changes to this type of building structure. If a similar building type is used, infill walls must be connected to the frame members, and a gap must be provided to allow the columns and girders to bend and form plastic hinges where they are designed and detailed to occur for seismic loading. Bricks and masonry blocks must also be connected to each other to prevent them from falling to the street below or into the apartments.

In terms of geotechnical engineering, the reconnaissance team highlighted the necessity of further investigating widespread liquefaction that occurred in Iskenderun, systematic monitoring of earth dams to identify the mechanisms that played a role in those damaged during the earthquakes and those that performed well, investigation of slope instability in Altinozu, Hatay for progressive failure potential, and site amplifications in various districts. Moreover, the exceedance of the TEBC (2019) design spectrum for the return period of 2475 years by response spectra of recorded motions at aforementioned stations should be further assessed in future studies.

It is important to note that the authors' conclusions are preliminary, and future research on the collected data will provide greater insight, as well as more definitive conclusions on the presented observations.

9   REFERENCES

ACI 318 (2005). Building Code Requirements for Structural Concrete (ACI 318-05) and Commentary (ACI 318R-05), ACI Committee 318, American Concrete Institute, Farmington Hills, MI.

Akansel, V.H, & Ozkula, G. (2021). The 30 October 2020, Mw 6.6 Sisam (Samos) Earthquake: Interpretation of Strong Ground Motions and Pos-Earthquake Condition of Nearby Structures. *European Jour. of Eng. and Applied Sci.*, 4(2), 66-86.

Akkar, S., & Boore, D. M. (2009). On baseline corrections and uncertainty in response spectra for baseline variations commonly encountered in digital accelerograph records. Bulletin of the Seismological Society of America, 99(3), 1671-1690.

Caltrans Seismic Design Criteria (SDC) (2019) Version 2.0.

Caltrans Seismic Design Criteria (SDC) (2006) Version 1.4.

Carlson, J.W., & Holmes, T. (2003). Silo failures: Why do they happen? *TASK Q.,* 7, 499-512.

Cetin et al. (2023). Preliminary Reconnaissance Report on February 6, 2023, Pazarcık M_w=7.7 and Elbistan M_w =7.6, Kahramanmaraş-Türkiye Earthquakes. METU Earthquake Engineering Research Center.

Cetin, H., Güneyli, H., & Mayer, L. (2003). Paleoseismology of the Palu–Lake Hazar segment of the East Anatolian fault zone, Türkiye. Tectonophysics, 374(3-4), 163-197.

Competing Against Time: Report to Governor Deukmejian from the Governor's Board of Inquiry on the 1989 Loma Prieta earthquake, 1989.

Converse, A. M., & Brady, A. G. (1992). Basic Strong-Motion Accelerogram Processing Software Version 1.0.

Doerich, C., & Rotter, J.M. (2008). Behavior of cylindrical steel shells supported on local brackets. *J. Struct. Eng.,* 134, 1269-1277.

Dowell, R.K., (2004) Time-History Analyses versus Measured Seismic Responses of the 5/14 Connector Bridge, Report (DH-04-02) to the Strong Motion Instrumentation Program, California Geological Survey, from Dowell-Holombo Engineering.

Hancilar, U., Sesetyan, K., Cakti, E., Safak, E., Yenihayat, N., Malcioglu, F. S., Donmez, K., Tetik, T., Suleyman, H. (2023). Kahramanmaraş-Gaziantep Türkiye M7.7 Earthquake, 6 February 2023 (04:17 GMT+03:00) Strong Ground Motion and Building Damage Estimations Preliminary Report (v6).

Hashash, Y. M. A., Musgrove, M. I., Harmon, J. A., Ilhan, O., Xing, G., Numanoglu, O., & Park, D. (2020). DEEPSOIL 7.0, User Manual. Board of Trustees of University of Illinois at Urbana-Champaign. Urbana.

Lin, J.L., Kuo, C.H., Chang, Y.W., Chao, S.H., Li, Y.A., Shen, W.C., Yu, C.H., Yang, C.Y., Lin, F.R., Hung, H.H., Chen, C.C., Su, C.K., Hsu, S.Y., Lu, C.C., Chung, L.L., and Hwang, S.J. (2020), "Reconnaissance and learning after the February 6, 2018, earthquake in Hualien, Taiwan", *Bulletin of Earthquake Engineering*, 18(10): 4725–4754.

Ministry of Environment and Urbanization of Türkiye (2023) , https://hasartespit.csb.gov.tr/

Saatcioglu, M., et al. (2001). The August 17, 1999 Kocaeli (Türkiye) earthquake – Damage to structures. *Can, J, Civ. Eng.*, 28(4), 715-773.

Seed, H. B., Romo, M. P., Sun, J. I., Jaime, A., Lysmer, J. (1988). The Mexico earthquake of September 19, 1985— Relationships between soil conditions and earthquake ground motions. Earthquake spectra, 4(4), 687-729.

Selcuk (1985). Kızıldağ–Keldağ–Hatay dolayının Jeolojisi ve Jeodinamik evrimi, M.T.A Rapor No 7787, Ankara. (in Turkish)

Şeşetyan, K., Stucchi, M., Castelli, V., & Gómez Capera, A. A. (2023). Kahramanmaraş-Gaziantep Türkiye M7. 7 Earthquake, 6 February 2023 (04: 17 GMT+ 03: 00) Large historical earthquakes of the earthquake-affected region: a preliminary report.

Priestley, M.J.N., Seible, F., & Calvi, G.M., Seismic Design and Retrofit of Bridges, John Wiley and Sons, New York, 1996.

Taskesen-Ozturk, G., Analysis of spatio-temporal changes of precipitation to estimate R factor in RUSLE at Kartalkaya Dam. MSc Thesis, Middle East Techncial University, Ankara, Türkiye. 84 pg.

TEBC (2019). Turkish Building Earthquake Code; *T.C. Resmi Gazete:* Ankara, Türkiye.

The Continuing Challenge: Report on the Northridge Earthquake to the Director, Department of Transportation, State of California, by the Seismic Advisory Board, 1994.

USGS (2023a). https://earthquake.usgs.gov/earthquakes/eventpage/us6000jllz/executive

USCS (2023b). https://earthquake.usgs.gov/earthquakes/eventpage/us6000jlqa/executive

Yuksel A, Gundogan R, Akay AE. (2008) Using the Remote Sensing and GIS Technology for Erosion Risk Mapping of Kartalkaya Dam Watershed in Kahramanmaras, Türkiye. *Sensors*; 8(8):4851-4865.

50 Years Later, an Earthquake's Legacy Continues, USGS, (2021). Communications and Publishing.